



Published in final edited form as:

Cell Rep. 2019 November 12; 29(7): 1789–1799.e6. doi:10.1016/j.celrep.2019.10.030.

Sam68 Enables Metabotropic Glutamate Receptor-Dependent LTD in Distal Dendritic Regions of CA1 Hippocampal Neurons

Matthew E. Klein^{1,8}, Thomas J. Younts^{1,9}, Carmen Freire Cobo^{1,10}, Adina R. Buxbaum^{3,7}, Jonathan Aow^{7,11}, Hediye Erdjument-Bromage⁴, Stéphane Richard⁵, Roberto Malinow⁷, Thomas A. Neubert⁴, Robert H. Singer^{1,3,6}, Pablo E. Castillo¹, Bryen A. Jordan^{1,2,12,*}

¹Dominick P. Purpura Department of Neuroscience, Albert Einstein College of Medicine, Bronx, New York, NY 10461, USA

²Department of Psychiatry and Behavioral Sciences, Albert Einstein College of Medicine, Bronx, New York, NY 10461, USA

³Department of Anatomy and Structural Biology, Albert Einstein College of Medicine, Bronx, New York, NY 10461, USA

⁴Department of Cell Biology and Kimmel Center for Biology and Medicine, Skirball Institute of Biomolecular Medicine, New York University School of Medicine, New York, NY 10016, USA

⁵Segal Cancer Center, Lady Davis Institute for Medical Research and Departments of Oncology and Medicine, McGill University, Montréal, QC H3T 1E2, Canada

⁶Janelia Research Campus of the Howard Hughes Medical Institute, Ashburn, VA 20147, USA

⁷Center for Neural Circuits and Behavior, Department of Neuroscience and Section for Neurobiology, Division of Biology, University of California at San Diego, San Diego, CA 92093, USA

⁸Present address: Department of Psychiatry, University of California at San Diego, San Diego, CA 92093, USA

⁹Present address: Department of Neuroscience, Physiology and Pharmacology, University College London, Gower Street London WC1E 6BT, UK

¹⁰Present address: Nash Family Department of Neuroscience, Icahn, Mount Sinai School of Medicine, New York City, NY 10029, USA

¹¹Present address: Genome Institute of Singapore, Singapore 138672, Singapore

This is an open access article under the CC BY-NC-ND license (<http://creativecommons.org/licenses/by-nc-nd/4.0/>).

*Correspondence: bryen.jordan@einstein.yu.edu.

AUTHOR CONTRIBUTIONS

Conceptualization, M.E.K., T.J.Y., P.E.C., and B.A.J.; Methodology, M.E.K., T.J.Y., H.E.-B., T.A.N., P.E.C., R.H.S., and B.A.J.; Investigation, M.E.K., T.J.Y., H.E.B., and B.A.J.; Writing – Original Draft, M.E.K., T.J.Y., P.E.C., and B.A.J.; Writing – Review & Editing, M.E.K., T.J.Y., P.E.C., and B.A.J.; Funding Acquisition, S.R., R.H.S., P.E.C., T.A.N., and B.A.J.; Resources, H.E.-B., S.R., P.E.C., and B.A.J., Supervision, P.E.C. and B.A.J.

DECLARATION OF INTERESTS

The authors declare no competing interests.

SUPPLEMENTAL INFORMATION

Supplemental Information can be found online at <https://doi.org/10.1016/j.celrep.2019.10.030>.

¹²Lead Contact

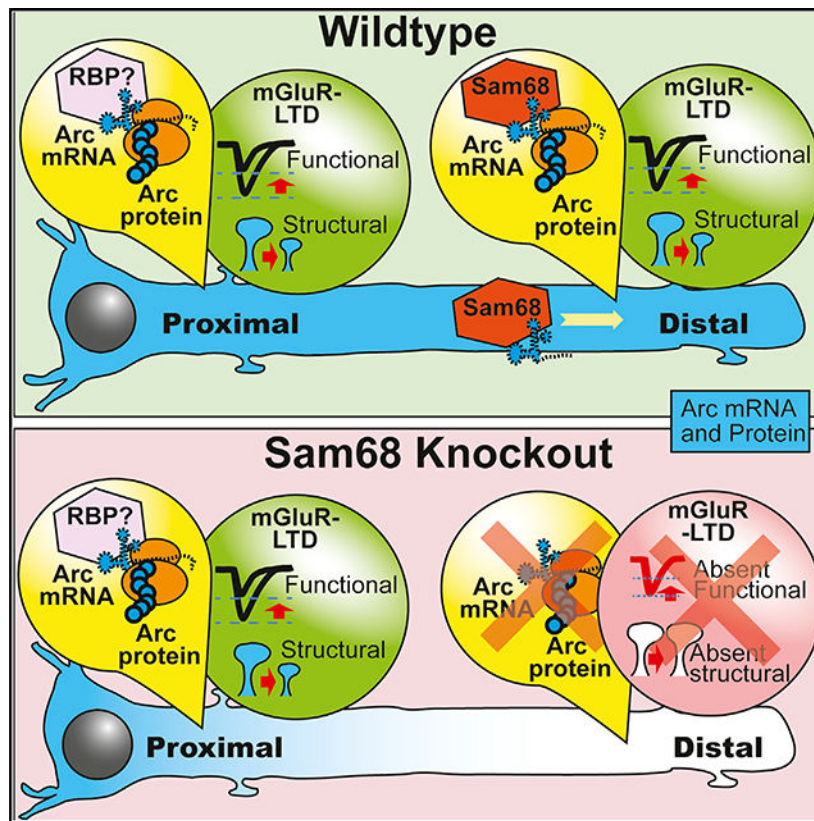
SUMMARY

The transport and translation of dendritic mRNAs by RNA-binding proteins (RBPs) allows for spatially restricted gene expression in neuronal processes. Although local translation in neuronal dendrites is now well documented, there is little evidence for corresponding effects on local synaptic function. Here, we report that the RBP Sam68 promotes the localization and translation of Arc mRNA preferentially in distal dendrites of rodent hippocampal CA1 pyramidal neurons. Consistent with Arc function in translation-dependent synaptic plasticity, we find that Sam68 knockout (KO) mice display impaired metabotropic glutamate-receptor-dependent long-term depression (mGluR-LTD) and impaired structural plasticity exclusively at distal Schaffer-collateral synapses. Moreover, by using quantitative proteomics, we find that the Sam68 interactome contains numerous regulators of mRNA translation and synaptic function. This work identifies an important player in Arc expression, provides a general framework for Sam68 regulation of protein synthesis, and uncovers a mechanism that enables the precise spatiotemporal expression of long-term plasticity throughout neurons.

In Brief

Although local translation in neuronal dendrites is well documented, there is little evidence for corresponding effects on local synaptic function. Klein et al. demonstrate that Sam68 is required for Arc protein synthesis at distal dendritic regions and is required for synaptic plasticity exclusively at distal dendrites of hippocampal pyramidal neurons.

Graphical Abstract



INTRODUCTION

Temporally and spatially regulated neuronal gene expression is fundamental for synaptic plasticity and high-order brain functions (for recent reviews see Biever et al., 2019; Donlin-Asp et al., 2017; Sossin and Costa-Mattioli, 2019; and Van Driesche and Martin, 2018). In neurons, global (Cajigas et al., 2012) and cell-type-specific (Ainsley et al., 2014; Kratz et al., 2014) RNA sequencing experiments have identified thousands of mRNAs in distal dendritic compartments. Classic and novel visualization methods, including SunTAG (Aakalu et al., 2001; Tanenbaum et al., 2014; Wang et al., 2016, 2009; Wu et al., 2016; Yoon et al., 2016), confirm that distally localized mRNAs and polysomes are translationally competent. Moreover, proteomic studies reveal that dendritic proteomes are mainly synthesized from dendritically localized mRNAs (Hodas et al., 2012; Zappulo et al., 2017). These findings indicate that mRNA transport and translation help shape the local neuronal proteome and corroborate long-standing evidence that dendritic protein synthesis is required for certain forms of synaptic plasticity (Kang and Schuman, 1996; Reymann and Frey, 2007; Wang et al., 2009). RNA-binding proteins (RBPs), such as Staufen (Heraud-Farlow and Kiebler, 2014), ZBP1 (Wu et al., 2015; Yoon et al., 2016), and FMRP (Darnell and Klann, 2013), transport and translate mRNAs within dendritic arbors and are required for long-lasting forms of synaptic plasticity. The loss of RBP function leads to numerous neurodegenerative and developmental disorders, including autism spectrum disorders (ASDs), fragile X syndrome (FXS) (Bhakar et al., 2012; Darnell and Klann, 2013; Jung et

al., 2014; Lee et al., 2016; Popovitchenko et al., 2016; Zoghbi and Bear, 2012), and intellectual disabilities and epilepsy (Lee et al., 2016; Zhao, 2013). Despite widespread interest in local gene expression, there is little evidence that localized deficits in protein synthesis lead to corresponding deficits in local neuronal function.

Sam68 is a multifunctional RBP with established roles in mRNA transport (Klein et al., 2013; Li et al., 2002; Modem et al., 2005), translation (Grange et al., 2009; Klein et al., 2013, 2015; Paronetto et al., 2009), and alternative splicing (Chawla et al., 2009; Iijima et al., 2011; Matter et al., 2002). Reduced Sam68 function has been linked to fragile X tremor ataxia syndrome (FXTAS) (Sellier et al., 2010), a relatively common neurodegenerative disorder associated with working memory impairments, mood instability, and progressive cognitive decline (Berman et al., 2014; Tassone et al., 2012). We recently found that Sam68 controls hippocampal synaptic plasticity by regulating the expression of activity-regulated cytoskeleton-associated protein (Arc) (Klein et al., 2015). Arc is an essential immediate early gene that is rapidly synthesized (Niere et al., 2012; Park et al., 2008) and degraded (Rao et al., 2006; Soulé et al., 2012), producing a discrete temporal window for the induction of translation-dependent forms of synaptic plasticity, such as metabotropic glutamate-receptor-dependent long-term depression (mGluR-LTD) (Klein et al., 2015; Park et al., 2008; Waung et al., 2008). The loss of Arc inhibits memory formation and produces behavioral deficits in rodents (Bramham et al., 2010; Greer et al., 2010; Rudinskiy et al., 2012), and Arc overexpression is sufficient to restore synaptic plasticity in juvenile mice and extend the critical period of visual cortical plasticity (Jenks et al., 2017). Notably, newly synthesized Arc mRNA is transported and translated near recently activated synapses (Farris et al., 2014; Moga et al., 2004; Steward et al., 1998; Steward and Worley, 2001) by unknown mechanisms. Here, we report that Sam68 regulates Arc mRNA translation and localization selectively at distal Schaffer collateral synapses of CA1 hippocampal pyramidal neurons and that Sam68 KO mice display impaired plasticity exclusively at distal synapses. Moreover, we elucidate the Sam68 interactome and provide mechanistic insights linking Sam68 to neuronal mRNA transport and translation.

RESULTS

Sam68 Regulates the Expression of Arc mRNA in Distal Dendrites of CA1 Hippocampal Neurons

Sam68 is required for mGluR-LTD (Klein et al., 2015), a form of synaptic plasticity that requires synthesis of the Arc protein (Park et al., 2008; Waung et al., 2008). To test whether Sam68 regulates Arc mRNA expression, we used RNAscope-based fluorescence *in situ* hybridization (FISH) to image Arc mRNA (Farris et al., 2014) in acute hippocampal slices following unilateral *in vivo* injections of adeno-associated virus (AAV) expressing Sam68-specific short hairpin RNAs (shRNAs) (shS68) or nontargeting shRNAs (shNTs) (Figure 1A). Western blots of microdissected hippocampal tissue confirmed that previously validated shRNA shS68 (Klein et al., 2013, 2015) reduced Sam68 protein levels (Figure 1B), and RNA immunoprecipitation (IP) confirmed that Sam68 associates with Arc mRNA (Grange et al., 2009) but not with non-cargo CaMKII α or MAP2 mRNAs (Figure 1C). We found that Sam68 knockdown decreased the amount of Arc mRNA in dendritic layers of

hippocampal *stratum (s.) radiatum* and increased the amount in the somatic layer (Figure 1D). We quantified these changes by measuring the % difference in mRNA enrichment between the ipsilateral (shS68- or shNT-injected) hippocampus and uninjected contralateral side (Figure 1E). Sam68 knockdown shifted the distribution of Arc mRNA toward the soma and proximal dendrites, resulting in a significant decrease in Arc mRNA in distal dendritic regions (Figure 1E, left panel). No difference in non-cargo CaMKII α mRNA distribution was observed in mice injected with either shS68 or shNT AAVs (Figure 1E, right panel). Cumulative mRNA distribution plots show similar results (Figure 1F). Arc mRNA distribution in heterozygous Sam68 KO mice (HET), which express ~50% of Sam68 protein levels found in wild-type (WT) littermates (Richard et al., 2008), showed a similar somatic shift in Arc mRNA distribution (data not shown).

To test whether Sam68 helps localize Arc mRNA through RNA degradation (Farris et al., 2014), we measured Arc mRNA stability by using qRT-PCR in primary hippocampal neurons following transcriptional inhibition using actinomycin D. Arc mRNA half-life following Sam68 knockdown was similar to control levels and similar to previously determined values (Rao et al., 2006), showing that Sam68 had no effect on Arc mRNA decay (Figure 1G). To determine whether Sam68 could regulate the dendritic transport of Arc mRNA, we tested whether Sam68 could interact with kinesin molecular motors, such as KIF5A, which regulates mRNA transport in neuronal dendrites (Hirokawa et al., 2010). Co-immunoprecipitations from cortical lysates revealed that Sam68 associates with kinesin KIF5A but not KIF17 or KIF1b (Figure 1H). These data strongly suggest that Sam68 is required for the distal localization of Arc mRNA in CA1 hippocampal neurons and may actively regulate mRNA transport by KIF5A.

Sam68 Regulates Arc mRNA Translation

To determine whether the loss of distal Arc mRNA led to reduced distal Arc protein, we performed immunostaining experiments. Due to high background observed in acute hippocampal slices (data not shown), we measured Arc protein distribution in cultured primary hippocampal neurons at days *in vitro* (DIV) 17–25 following stimulated activity (KCl; 60 mM, 10 min) to induce Arc translation (Kim et al., 2010; Zheng et al., 2009). Consistent with mRNA imaging in acute hippocampal slices, Sam68 knockdown preferentially decreased Arc protein >100 μ m from the cell body (Figure 2A). No changes in Arc expression were observed near the cell body (<25 μ m) (% Arc compared to levels in cell body; <25 μ m shNT = 71.8% \pm 2.4%, shS68 = 69.4% \pm 2.4%; >100 μ m shNT = 22.3% \pm 0.14%, shS68 = 13.6% \pm 0.11%). Fluorescent non-canonical amino acid tagging (FUNCAT) using puromycylation revealed no changes in overall protein synthesis following Sam68 knockdown (Figure 2B). Moreover, Sam68 knockdown had no effect on Arc protein half-life, as measured in primary neuronal cultures treated with the translational inhibitor cycloheximide (Figure 2C).

We and others have shown that Sam68 helps load mRNA cargos onto polysomes and regulates protein abundance (Grange et al., 2009; Klein et al., 2013, 2015; Paronetto et al., 2009). To test whether Sam68 directly regulates mRNA translation, we performed rabbit-reticulocyte-lysatebased *in vitro* translation assays using synthesized Arc mRNA as a

template and purified GST-Sam68. Adding Sam68 resulted in a dose-dependent increase in Arc protein synthesis (Figure 2D). Statistically significant results were observed at 100 ng of purified Sam68-GST protein, corresponding to ~50 nM Sam68. GST protein alone had no effect on basal Arc protein synthesis. These results show that Sam68 can directly regulate the translation of Arc mRNA.

Sam68 Regulates mGluR-LTD Exclusively at Distal CA1 Synapses

To examine the functional implications of reduced dendritic Arc mRNA/protein, we measured mGluR-LTD, a form of long-term synaptic plasticity that requires Arc protein synthesis (Klein et al., 2015; Park et al., 2008; Waung et al., 2008), along the somatodendritic axis of pyramidal neurons in acute hippocampal slices. We measured mGluR-LTD at excitatory Schaffer collateral inputs onto CA1 pyramidal cells (Sch-CA1) by using extracellular field potential recordings from proximal (~40 μ m) and distal inputs (~150 μ m) relative to the cell body layer, avoiding the more distal perforant pathway in *s. lacunosum moleculare*. Experiments were performed under conditions (see STAR Methods) where mGluR-LTD is observed to be dependent on protein synthesis (Klein et al., 2015; Younts et al., 2016). In WT mice, the magnitude of Dihydroxyphenylglycine (DHPG)-induced mGluR-LTD (50 μ M, 5 min) was similar between proximal and distal inputs (Figure 3A, left panel). As we showed previously (Klein et al., 2015), homozygous Sam68 KO mice displayed severely impaired mGluR-LTD in distal dendritic inputs (Figure 3A, right panel). Surprisingly, mGluR-LTD at proximal inputs were normal in Sam68 KO mice (% LTD; WT proximal = 65.2% \pm 3.3%, KO proximal = 68.5% \pm 4.3%, WT distal = 61.6% \pm 4.2%, KO distal = 90.6% \pm 6.1%). Like homozygotes, HET Sam68 KO mice also displayed impaired mGluR-LTD only at distal synapses (% LTD; HET proximal = 71.3% \pm 2.7%, HET distal = 84.9% \pm 3.9%) (Figure 3B), indicating that Sam68 haploinsufficiency was enough to induce localized deficits in synaptic plasticity.

In addition to chemically induced mGluR-LTD, we measured synaptically induced mGluR-LTD. As before, pipettes placed in distal or proximal *s. radiatum* were used to trigger synaptic mGluR-LTD by using a well-established paired pulse low-frequency stimulation (PP-LFS) induction protocol (Huber et al., 2000). No differences were observed along the somatodendritic axis in WT mice (% LTD; WT proximal = 67.6% \pm 5.7%, WT distal = 63.8% \pm 2.9%) (Figure 3C, left panel). However, similar to chemical induction, synaptically induced mGluR-LTD was impaired only at distal synapses in HET mice (% LTD; HET proximal = 78.1% \pm 1.8%, HET distal = 110.0% \pm 3.2%) (Figure 3C, right panel). Together, these results confirm that Sam68 preferentially regulates mGluR-LTD at distal synapses of CA1 hippocampal neurons.

To explore how mGluR-LTD was normal at proximal inputs in Sam68 KO mice, we tested whether somatic Arc or other somatic compensatory factor(s) could diffuse into proximal dendritic inputs to restore LTD. To assess this possibility, we measured DHPG-induced mGluR-LTD at proximal synapses following surgical transection of the soma from pyramidal cell dendrites. Consistent with our prediction, mGluR-LTD was abolished in isolated proximal dendrites of Sam68 KO mice (Figure 3D). This effect was not due to the transection itself, as this manipulation had no significant effect on LTD at proximal synapses

in WT mice (% LTD; KO cut = $107.3\% \pm 4.7\%$, WT cut = $80.4\% \pm 0.25\%$, KO intact = $72.5\% \pm 4.4\%$). These data suggest that Arc synthesized by alternative mechanisms in CA1 pyramidal cell somata may normally contribute to mGluR-LTD in proximal dendrites.

LTD induction leads to a protein-synthesis-dependent reduction in dendritic spine size and number (Nägerl et al., 2004; Oh et al., 2013; Ramiro-Cortés and Israely, 2013; Wang et al., 2007; Zhou et al., 2004). To determine whether we could observe corresponding localized deficits in mGluR-dependent structural plasticity, we used two-photon fluorescence imaging of neurons in organotypic slices. We introduced either shS68 or shNT into CA1 pyramidal cells using single-cell electroporation through a patch pipette and measured dendritic spine morphology 7 days post-transfection (Figure 4A). Consistent with previous studies (Oh et al., 2013; Ramiro-Cortés and Israely, 2013), DHPG stimulation ($50 \mu\text{M}$, 5 min) reduced spine diameter in both proximal and distal regions of neurons expressing shNT (diameter [% baseline]; shNT distal = $80.4\% \pm 4.4\%$, shNT proximal = $83.2\% \pm 4.5\%$). In contrast, DHPG stimulation of neurons transfected with shS68 led to a decrease in spine diameter in proximal but not distal dendritic regions of CA1 pyramidal neurons (diameter [% baseline]; shS68 distal = $98.5\% \pm 3.2\%$, shS68 proximal = $82.2\% \pm 3.9\%$) (Figure 4B). Together, these results show that the loss of Sam68 leads to deficits in structural and functional plasticity exclusively in distal dendritic regions of CA1.

The Sam68 Interactome Reveals Multiple Regulators of mRNA Translation

To gain insight into the mechanisms linking Sam68 to Arc synthesis and synaptic function, we identified the Sam68 interactome by quantitative mass spectrometry by using a 10-plex set of isobaric tandem mass tags (Thompson et al., 2003). We performed 10 unique IPs from mouse brain lysates by using control, Sam68, and unrelated protein antibodies. Following high-resolution mass spectrometry, data analysis, normalization against unrelated protein interactomes, and the application of a high-stringency filter to reduce false positives (minimum 2 peptides identified; 2-fold enrichment), we identified individual protein interactomes. As expected, the Sam68 replicate interactomes showed the greatest overlap (62%). A hypergeometric distribution analysis (probability density function) revealed that this overlap was several orders of magnitude more statistically significant than for other proteins (Figure 5C), suggesting a high-confidence set of Sam68 interactors. We found that Sam68 binds to other RBPs, as well as numerous splicing factors, regulators of translation, and synaptic proteins (Table S1). Network analyses (<https://string-db.org>) (Figure 5D) identified significantly more interactions than expected from a random protein set (protein-protein interaction enrichment p value = $1.0e^{-16}$), suggesting that Sam68 associates with established protein complexes. Expanding our stringency filter (> 1.5 -fold enrichment) (Table S2) revealed additional regulators of protein synthesis, splicing, and synaptic function. Ontological analyses of the Sam68 interactome suggest it is strongly associated with protein synthesis, ribosomal function, and splicing (Figure 5E; Table S3). Moreover, Sam68 interactions with kinesins KIF 2, 3, and 5 corroborate and extend our findings (Figure 1H) that Sam68 may regulate mRNA transport, whereas interactions with eukaryotic initiation factors eIF3 and eIF4 suggest that Sam68 promotes Arc protein synthesis at the level of translation initiation.

DISCUSSION

We provide evidence that Sam68 differentially regulates long-term synaptic plasticity along the somatodendritic axis of hippocampal CA1 pyramidal neurons. Specifically, we show that changes in the spatial distribution of Arc mRNA and protein lead to corresponding and spatially restricted changes in structural and functional plasticity. Our *in vitro* translation experiments indicate that Sam68 can directly promote translation of Arc mRNA, and proteomic analyses provide insights into potential mechanisms linking Sam68 to RNA transport and protein synthesis. Overall, these results identify an important regulator of the dendritic proteome that selectively affects functional and structural plasticity in distal dendritic regions of CA1 hippocampal neurons.

The observation that mGluR-LTD is normal in proximal dendritic regions in Sam68 KO mice suggests that a Sam68-dependent mechanism synthesizes Arc protein in dendrites, whereas a Sam68-independent mechanism synthesizes Arc protein at the soma. Because of diffusion, these two sources are likely redundant in proximal dendritic regions. This model is supported by our transection experiments, which show that removing the soma abolishes proximal mGluR-LTD in KO mice because of the loss of both Sam68-dependent and Sam68-independent mechanisms but not in WT mice because of redundancy from Sam68. This interpretation is further supported by our previous work that revealed that Arc protein can be synthesized through Sam68-independent mechanisms (Klein et al., 2015), as well as classical studies showing that Arc can be synthesized in the soma (Lyford et al., 1995; Steward et al., 1998). Alternative explanations based on potential compensation in KO mice are unlikely because we observed distal-specific plasticity deficits in Sam68 heterozygotes, as well as following shRNA knockdown. Therefore, we propose a model where redundant Sam68-dependent and independent pathways regulate Arc abundance and mGluR-LTD in proximal dendrites.

Interactions with kinesin proteins and *in vitro* translation assays suggest that Sam68 directly regulates Arc mRNA transport and translation. These effects were not observed for CaMKII α mRNA, and FUNCAT experiments show that the loss of Sam68 does not globally affect translation, suggesting specific activity. Previous screens for Sam68 mRNA cargos identified regulators of neuronal function and the cytoskeleton (Grange et al., 2009; Itoh et al., 2002). A systematic evolution of ligands by exponential enrichment experiment found that Sam68 preferentially binds to UAAA and poly(U) sequences (Itoh et al., 2002). Arc mRNA harbors two dendritic transport elements, as well as several A/U-rich regions that confer dendritic localization (Ninomiya et al., 2016), although it is not yet known if these are required for Sam68 binding. Although it is tempting to speculate that Sam68 directs Arc mRNA toward activated synapses, a previous study suggested that input-specific localization results from selective degradation of widely distributed Arc mRNA at inactive synapses (Farris et al., 2014). Because we found that Sam68 does not regulate Arc mRNA decay, we propose that Sam68 broadly distributes mRNAs into distal dendritic regions and that nonsense-mediated decay, which has been shown to control Arc mRNA levels (Giorgi et al., 2007), regulates selective expression at activated synapses.

Our robust and unbiased proteomic analyses of the Sam68 interactome provides important mechanistic insights into the multifunctional nature of Sam68. For example, we identified numerous splicing factors (U2AF2, SRSF3,7 and X-linked splicing factor hnRNP G [RBMX]), which give insight into the established role of Sam68 in alternative splicing (Chawla et al., 2009; Iijima et al., 2011, 2014; Matter et al., 2002). Relevant to protein synthesis, we found that Sam68 binds to diverse ribosomal components and to eukaryotic initiation factors eIF4G and eIF3. eIF3 is a multi-component complex that regulates translation initiation by controlling ribosome subunit assembly (Chiu et al., 2010; Jackson et al., 2010; Lee et al., 2008) and recruiting mRNAs to the 43S pre-initiation complex through interactions with eIF4G (des Georges et al., 2015; Hinnebusch, 2006). We speculate that Sam68 may regulate Arc translation initiation by promoting the association of Arc mRNA with pre-initiation complexes, which is consistent with previous findings showing that Sam68 promotes ribosomal loading (Grange et al., 2009; Klein et al., 2013; Paronetto et al., 2009).

Our study builds on previous work characterizing dendritic Arc mRNA transport and translation and the role of Arc protein synthesis in mGluR-LTD (Bramham et al., 2010; Farris et al., 2014; Moga et al., 2004; Park et al., 2008; Steward et al., 1998; Steward and Worley, 2001; Waung et al., 2008). Although reports suggest that Arc metabolism is also important for NMDA-receptor-dependent LTD (Plath et al., 2006), we found that neither chemically nor synaptically induced NMDA-dependent LTD was affected in Sam68 KO mice (Klein et al., 2015), suggesting a specificity for mGluR-LTD. We were unable to establish a causal link between the observed deficits in Arc mRNA transport and translation and the localized deficits in mGluR-LTD because methods to selectively restore Arc mRNA exclusively at distal dendrites are not available. Moreover, Arc levels would need to be restored to near-endogenous levels, as overexpressing Arc strongly decreases synaptic α -amino-3-hydroxy-5-methyl-4-isoxazolepropionic acid receptor expression and occludes mGluR-dependent LTD (Chowdhury et al., 2006; Waung et al., 2008).

Unlike the role of cerebellar mGluR-LTD in motor learning (Jörntell and Hansel, 2006; Kano et al., 2008), the role of hippocampal mGluR-LTD on behavior is less clear. Although no cognitive deficits were found in previous behavioral tests performed on Sam68 KO mice (Lukong and Richard, 2003, 2008), recent studies suggest that hippocampal mGluR-LTD may contribute to behaviors associated with spatial distribution of novel objects, a process not affected by hippocampal LTP (Kemp and Manahan-Vaughan, 2008; Mukherjee and Manahan-Vaughan, 2013). We propose that specialized and targeted behavioral analysis of Sam68 KO mice will provide a unique opportunity to determine how the loss of region-specific plasticity ultimately affects cognition. Taken together, our work provides a general framework for Sam68 regulation of protein synthesis, identifies molecular mechanisms underlying Arc synthesis, and increases our understanding of the spatiotemporal regulation of gene expression in neurons.

STAR★METHODS

LEAD CONTACT AND MATERIALS AVAILABILITY

Further information and requests for resources and reagents should be directed to and will be fulfilled by the Lead Contact, Bryen A. Jordan (bryen.jordan@einstein.yu.edu).

Materials Availability Section—Purified GST-coupled Sam68 protein and oligonucleotides generated in this study are freely available from the lead contact, provided sufficient stock levels. Bacterial expression plasmid used to generate Sam68 protein is available at Addgene as pGEX-2T-Sam68 (# 17687). Sam68 Knockout mice generated by Stéphane Richard have been deposited and are available at The Jackson Laboratory (JAX) as B6.129(C)-Khdrbs1tm1Rchd/J, with stock #018444.

EXPERIMENTAL MODEL AND SUBJECT DETAILS

Animals—Mice were housed and handled at the Albert Einstein College of Medicine (Bronx, NY) Janelia Research Campus (Ashburn, VA), and the University of California at San Diego (UCSD). All experiments were approved by and were in compliance with the Albert Einstein College of Medicine, Janelia Research Campus, and UCSD Institutional Animal Care and Use Committees. We used wild-type male or female C57BL/6J mice, heterozygous Sam68 knockout mice (HET), or homozygous Sam68 knockout mice (KO) (P21–P35) all bred into a C57BL/6J background.

Acute Hippocampal Slices—Mice were deeply anesthetized with isoflurane and then killed by decapitation. The brain was removed and quickly placed in ice-cold cutting solution containing the following (in mM): 215 sucrose, 20 glucose, 26 NaHCO₃, 4 MgCl₂, 4 MgSO₄, 1.6 NaH₂PO₄, 1 CaCl₂, and 2.5 KCl. Hippocampi were dissected and mounted on an agar block, and transverse slices 400 μm thick were prepared with a DTK-2000 microslicer (Dosaka EM). To reduce variability that can arise from biological differences across the dorsoventral axis of the hippocampus, electrophysiological recordings were performed on the middle 1/3 of the tissue (i.e., the middle 2 mm). Slices were placed in a holding chamber (pre-warmed to 30°C via hot water bath) containing 50% cutting solution and 50% artificial CSF (ACSF) recording solution containing the following (in mM): 124 NaCl, 26 NaHCO₃, 10 glucose, 2.5 KCl, 1 NaH₂PO₄, 2.5 CaCl₂, and 1.3 MgSO₄. After 30 min, the 1:1 solution was switched to ACSF at 30°C and the holding chamber was removed from the water bath. Slices recovered in ACSF at room temperature for at least 1 h, and then were transferred to a submersion-type, temperature-controlled recording chamber (TC-344B, Warner Instruments) and perfused with ACSF at 2 ml/min using a peristaltic pump (Dynamax RP-1, Rainin). Experiments were performed at 30°C. All solutions were equilibrated for at least 30 min with 95% O₂ and 5% CO₂, pH 7.4.

Primary and Organotypic Neuronal Cultures—Primary cortical and hippocampal cultures were prepared from E18–19 Sprague Dawley rat embryonic brain tissue by dissociation with trypsin. Neurons were plated onto poly-L-lysine coated coverslips in 12 or 24-well tissue culture plates at a density of 200–250 cells per mm². Cells were initially plated in Dulbecco's Modified Eagle Medium (DMEM) + 10% fetal bovine serum, 0.45%

glucose, 1 mM pyruvate, and antibiotics. After 1.5 hr, media was replaced with Neurobasal (GIBCO, Invitrogen) containing B27, 0.5 mM Glutamax (GIBCO, Invitrogen), and antibiotics. One third of the media was changed every 5–7 days. Neurons were typically infected with lentiviruses ~DIV5–10 and imaged or analyzed 1–2 weeks later. Rat organotypic hippocampal slice cultures from postnatal day 6–8 pups were generated using a tissue chopper, and plated on poly-L-lysine coated wells as described (Haas et al., 2001; Otmakhov and Lisman, 2012). Primary dissociated and organotypic cultures were generated from embryonic and/or young rats whose sex was not determined, so our cultures contain cells from both sexes.

METHOD DETAILS

Electrophysiology—Extracellular field recordings were performed using an Axon MultiClamp 700B amplifier (Molecular Devices). Signals were filtered at 2 kHz and digitized at 5 kHz. Stimulation and acquisition were controlled with custom software in Igor Pro 5 (Wavemetrics). Unbroken stimulating patch-type pipettes (intensity < 10 μ A, 200 μ square pulses) were filled with ACSF and placed in proximal CA1 *stratum (s.) radiatum* (within ~40 μ m of the cell body layer *s. pyramidale*) and/or distal *s. radiatum* (~150 μ m away from *s. pyramidale*), avoiding the anatomically distinct *s. lacunosum moleculare* that harbors synapses of the perforant pathway. A patch-type recording pipette (filled with 1 M NaCl) was also placed in *s. radiatum* at the same distance from the cell body layer as the stimulating pipette. The stimulating and recording pipettes were positioned close to each other (~100–150 μ m apart) at approximately the same depth in the tissue (~100 μ m). In a subset of experiments (data not shown), potential overlapping recruitment of synaptic inputs was assessed by testing whether stimulation of one subset of inputs (e.g., proximal or distal) altered the responses induced by activating the other inputs (e.g., distal or proximal, respectively) 40 ms later. No cross-talk was observed between inputs, strongly suggesting that proximal or distal inputs could be activated independently. To monitor changes in synaptic strength over time, stimuli were delivered at 0.1 Hz before (i.e., baseline), during, and after the induction of long-term plasticity. In the field experiments using DHPG, two independent pathways were recorded per slice, one on either side of the recording pipette, and the magnitude of plasticity averaged together per slice. For the paired pulse (PP) low frequency stimulation (LFS) experiments, a single pathway was stimulated and recorded. 50 μ M DL-APV, an NMDAR antagonist, was applied continuously throughout the experiment to block NMDAR-mediated plasticity. The PP-LFS protocol was 900 pulses at 1 Hz (total 15 minutes); each pulse consists of two stimuli with a 50 ms inter-stimulus interval (Huber et al., 2000). Synaptically and chemically-induced mGluR-LTD measured under the conditions described above and using acute hippocampal slices from 3–5 week old mice, is dependent on protein synthesis (Klein et al., 2015; Younts et al., 2016). All recordings were performed blind to mouse genotype. “n” values for slices and mice are reported in the figure legends. For statistical analyses, n = number of animals; thus, values used represent the average magnitude of plasticity for the pooled slices from each animal.

Antibodies, Oligos, and shRNAs—Antibodies used were: rabbit anti-Sam68 (sc-333, SCBT, 1:500); mouse anti-Sam68 (sc-136062 mouse: SCBT); mouse anti-puromycin (Clone 12D10; Millipore; 1:20,000); mouse anti-PSD95 (clone K28/43, UC Davis, NeuroMab

Facility 1:5000); chicken anti-MAP2 (EnCor Biotechnology, Cat# CPCA-MAP2); mouse anti-Arc (sc-17839, SCBT, 1:500); rabbit anti-Arc (156003, SYSY, 1:1000); mouse anti-RPS3 (sc-376098, SCBT, 1:1000); goat anti-KIF17 (Santa Cruz Biotechnology; 1:200) and mouse anti KIF5A (NKHC1, C-11, Santa Cruz Biotechnology; 1:200). RT-qPCR was performed on a CFX96 (BioRad) and iTaq Universal One-Step RT-qPCR (BioRad). Oligonucleotides used for RT-PCR were Arc (5'-ATGAATGGGCCAGCCAAGAA and 5'-TCCTCCTCAGCGTCCACATA), MAP2 (5'-CTGCCGGACCTGAAGAATGT and 5'-GCTTGGGGACTGTGTGATGA) and CaMKII α (5'-GAAGATGTGCGACCCTGGAA and 5'-TGCGGATATAGGCGATGCAG). shRNAs used for knockdown of Sam68 (shS68) targeted the 3' UTR of Sam68: (5'-GTTATGAG CAAACTTGTTACT) and a non-targeting (shNT) sequence (5'-GCGTCACCAATGCGTTAATGG) as described (Klein et al., 2013). Adenoviral associated virus serotype 2 was generated in the Janelia Research Campus core facility using the shRNA sequences above.

Arc Metabolism—To measure Arc protein turnover, we grew primary cortical neurons in a 12-well plate and transduced neurons with previously validated (Klein et al., 2013) lentivirally delivered control (shNT) or Sam68 specific (shS68) shRNAs at DIV 7 and blind to experimenter. At DIV 15 we treated neurons with freshly made cycloheximide (200 μ M) for different time points followed by lysis. Arc levels were then quantified using fluorescent western blotting (LI-COR Biosciences). To measure Arc mRNA degradation, we performed similar experiments but treated neurons with Actinomycin D (1 μ g/ml) at different time points followed by RNA extraction using RNeasy mini-kit (QIAGEN). RT-qPCR was performed using the oligos and the kits as described in the manufacturer's directions.

Protein and RNA Immunoprecipitations—P35–45 old Sam68 KO or WT mice were euthanized using CO₂ and cortex was quickly dissected and Dounce homogenized 20 times in lysis buffer: 25 mM Tris pH 7.4, 50 mM KCl, 5 mM EDTA, 0.5 mM DTT, 0.5% NP40 and 100 U/ml RNase inhibitor containing protease inhibitors cocktail (Thermo scientific). Lysates were incubated at 4°C with rocking for 1 hr and then centrifuged at 20,000 \times g for 30 min. 1 mg of WT or Sam68 KO lysate was incubated with 2 mg of Sam68 antibody overnight at 4°C and immunocomplexes recovered with protein G agarose preblocked with 5% BSA/PBS and salmon sperm DNA. Protein Co-IPs were processed by standard methods and elutions were analyzed by western blot. For RNA immunoprecipitations (RIPs), beads were treated with proteinase K for 10 min, and RNA was eluted using the Trizol method and nucleic acids were precipitated in the presence of glycogen. RT-PCR was performed using the oligos described above.

Single-Cell Electroporation and Two-Photon Microscopy—CA1 neurons from 6–8 DIV rat organotypic hippocampal slices were single-cell electroporated following a previously established protocol (Haas et al., 2001; Otmakhov and Lisman, 2012). An expression plasmid containing either shS68 or shNT shRNAs in addition to GFP was diluted to a final concentration of ~200 ng/ μ l with Ringer solution containing 2 mM Ca²⁺ and 12 mM Mg²⁺ and loaded into a glass patch pipette of ~4 MOhm resistance. An organotypic slice (resting on the porous membrane it was grown on) was placed in a 35 mm dish filled with filter-sterilized Ringer solution and visualized under a 60x objective without

superfusion. Electroporation was performed by guiding the patch pipette in close apposition to a pyramidal cell under positive pressure, followed by removal of pressure and application of a series of voltage pulses (1 ms, 200Hz, ~5V) for 500 ms using a Master 8 pulse generator (A.M.P.I., Israel). Typically, ~5 neurons were electroporated per slice. Slices were then returned to the incubator and maintained for an additional ~3–5 days before LTD experiments. Imaging was performed as described (Dore et al., 2015) and using a SliceScope two-photon microscope (Scientifica) equipped with a 60x water-immersion objective (LUMPLFLN 60XW, NA = 1.0; Olympus). A Chameleon Ultra II IR laser (Coherent) (80-MHz repetition rate, 100- to 150-fs pulses) tuned at 930 nm (2p) was used for the excitation of GFP. Fluorescence emission was detected with a hybrid PMT detector (HPM-100–40, Becker and Hickl) between 490 and 540 nm by means of a GFP emission filter (ET 515/50, Chroma). Organotypic slices were placed in a perfusion chamber in the microscope and allowed to acclimate for 10 minutes. After this period both proximal and distal dendritic regions of apical dendrites on CA1 pyramidal neurons were imaged. DHPG (50 μ M) was added to the perfusate for 5 minutes to induce mGluR-LTD, before being washed out. The same dendritic regions were reimaged 30 min later. Spines were visualized by GFP fluorescence, and diameter measurements were performed using the full-width half-maximum measurement (FWHM), a measurement independent of fluorescence intensity, as described (Ramiro-Cortés and Israely, 2013). ImageJ (NIH) was used to draw ROI's around spines in the pre-LTD images and to fit a Gaussian distribution to a plot of fluorescence intensity. FWHM was measured from this Gaussian fit. ROI's were then transferred to the post-LTD images and FWHM was again measured.

Arc mRNA and Sam68-GST Synthesis and *In Vitro* Translation—Sam68-GST was purified as described (Lin et al., 1997) and generated using pGEX-2T Sam68, which was a gift from David Shalloway (Addgene plasmid # 17687). Briefly, BL21 E. Coli transformed with Sam68-GST or GST alone, were induced using 0.5 mM IPTG at 30°C for 4 hours. Protein was then purified using standard conditions using glutathione beads and dialyzed following elution, prior to storage at –20°C in 50% glycerol. Arc mRNA was synthesized using a T3 transcription kit (New England Biolabs) using full-length *Mus musculus* Arc cDNA containing the 3' and 5' UTR. For *in vitro* translation, we used a rabbit reticulocyte system (Promega), using no mRNA as a control and 0.2 μ g of mouse Arc mRNA including mus Arc 3' and 5' UTR in 10 μ l reactions for testing. Purified Sam68-GST or GST protein were added to the reactions at the indicated amounts.

Immunocytochemistry, FUNCAT/Puromycylation—Primary hippocampal neurons were transduced with lentiviral shRNAs that also expressed eGFP at DIV 5–7 and blind to experimenter. For immunocytochemistry, neurons at DIV 17–25 were then fixed with 4% PFA/PBS for 5 min and immunostained for Arc or MAP2. For FUNCAT using puromycin, neurons at DIV 17–25 were treated with 10 μ M puromycin for 15 min prior to fixation and washing cells using 0.0025% digitonin to extract free puromycin. Neurons were immunostained using mouse anti-puromycin antibodies using standard protocols. The intensity of Arc or Puromycin staining was measured in GFP positive neurons and plotted as function of distance from the soma as shown using ImageJ (NIH).

In Vivo AAV-shRNA Injections and RNA Scope—Adeno-associated virus serotype 2 was produced by Janelia Research Campus viral core, expressing GFP and an shRNA either targeting Sam68 (shS68) *sense* 5′-CGT TAT GAG CAA ACT TGT TAC T-3′ *antisense* 5′-AGT AAC AAG TTT GCT CAT AAC T-3′ or a non-targeting control (shNT) *sense* 5′-AAG TAT CTA AGC TGT CAC AGA T-3′ *antisense* 5′-ATC TGT GAC AGC TTA GAT ACT C-3′. Unilateral hippocampal injections were performed on 4-week old mice, and virus was allowed to express for two weeks before animals were sacrificed and brains sectioned at 20 μm on a cryostat. Sections were mounted on slides and stored frozen at -80°C until used for fluorescent *in situ* hybridization (FISH). Single molecule FISH experiments were carried out with RNAscope technology per manufacturers protocols for multiplexed fluorescence assays with paraformaldehyde fixed, frozen brain tissue (<https://acdbio.com>). The probes used were RNAscope-Probe-Mm-Arc and RNAscope-Probe-Mm-Camk2a. To increase detection of Arc mRNA (Jakkamsetti et al., 2013; Steward et al., 2015), we exposed mice to an enriched environment using toys and novel objects for 30 minutes immediately prior to transcardial perfusion and sacrifice. Sam68 knockdown resulted in a small, but non-significant decrease in total Arc and CaMKIIα mRNA levels (Arc mRNA count; shS68 Ipsi = 2,290 ± 592, shS68 Contra = 3,567 ± 520, shNT Ipsi = 3,883 ± 487, shNT Contra = 4,217 ± 592; 2-way ANOVA Hemisphere (F = 0.39, p = 0.6), AAV (F = 0.11, p = 0.80); CaMKIIα mRNA count; shS68 Ipsi = 7,653 ± 1084, shS68 Contra = 9,870 ± 780, NT Ipsi = 9,463 ± 672, shNT Contra = 10,749 ± 745; 2-way ANOVA Hemisphere (F = 96, p = 0.06), AAV (F = 42, p = 0.09)). Sam68 Heterozygous KO mice showed no statistically significant change in total Arc mRNA (Total Arc mRNA count; WT = 2,998 ± 146, HET = 3,162 ± 154; t test p = 0.46).

Multiplexed Large-Scale Immunoprecipitations—To perform immunoprecipitations (IP), we incubated 300 μg of antibodies with 200 μl of protein G-Sepharose beads for 1hr at 4°C in PBS, washed 2X with 0.2 M triethanolamine pH 8.2 (TEA), and then crosslinked using freshly made 30 mM dimethyl pimelimidate (DMP) in TEA for 25 min at RT. Beads were washed for 5 min with TEA, crosslinked again using a fresh DMP solution, washed 3X with TEA, and finally quenched using two 10 min washes of 100 mM ethanolamine. Unbound antibodies were stripped off beads 3X using 100 mM glycine at pH 3.1 for 5 min, and beads were then washed 2X with PBS and stored in PBS/NaN₃. For crosslinking antibodies to magnetic beads, we coupled 90 μg of antibodies to 6 mg of Epoxy-Dynabeads (Dyna) according to the manufacturer's instructions. Each coupling reaction (Sepharose or epoxy) contained a mixture of rabbit and mouse antibodies (1/2 each of the total) for that specific antigen. The antibodies used were: control = normal rabbit IgG + normal mouse IgG, Sam68 = rabbit anti-Sam68 (sc-333; SCBT) + mouse anti-Sam68 (sc-136062 mouse: SCBT), and rabbit and mouse antibodies for remaining unrelated proteins. Each individual IP was split into two reactions: One IP consisted of ~40 μg of coupled antibodies incubated with 5 mg of total mouse brains lysed in a gentle dodecyl-β-maltoside buffer (DBM: 10 mM HEPES pH 7.4, 190 mM NaCl, 10 mM KCl, 1 mM EGTA, 1% Dodecyl-β-Maltoside), and the second IP consisted of ~40 μg incubated with 5 mg of mouse brains lysed in a harsher RIPA buffer (25 mM Tris pH 7.4, 300 mM NaCl, 1% Triton X-100, 0.5% deoxycholate, 0.1% SDS and 2 mM EDTA). This approach allowed for the capture of detergent sensitive interactions (DBM), and additional interactions (RIPA) present in detergent resistant synaptic and nuclear structures. We incubated IPs for 2 hours at RT with rocking, and then

added two volumes of either 10 mM HEPES for DBM lysates, or 25 mM Tris for RIPA lysates, to dilute salts and detergents, and incubated overnight at 4°C. Beads were then washed 5X with TBS/Tween-20, both DBM and RIPA IPs for each antigen were mixed, and finally eluted in 2X non-reducing Laemmli sample buffer at 70°C for 30 minutes.

Tandem Mass Tag (TMT) Labeling of Peptides—10 µg of each affinity enriched sample was electrophoresed briefly (dye front approximately 5mm) into a 15% SDS-PAGE gel. The gel was washed 3x in ddH₂O for 15 min each and visualized by staining overnight with GelCode® Coomassie blue reagent (Pierce). The stacked protein bands were excised from the gel and reduced with DTT and alkylated with iodoacetamide. In-gel digestion was performed using 5 ng/µL mass spectrometry grade trypsin (Trypsin Gold, Promega, Madison, WI, USA) in 50 mM NH₄HCO₃ digest buffer. The resulting peptides were desalted using a Stage Tip manually packed with Empora C18 High Performance Extraction Disks (3M, St. Paul, MN, USA) (Rappsilber, 2007) and eluted peptide solutions dried under vacuum. Peptides were then re-suspended in 18 µL acetonitrile and to each, 57 µL of 0.2 M HEPES buffer, pH 8.5 added. TMT10-plex amine reactive reagents (5 mg per vial) (Thermo Fisher Scientific) were re-suspended in 1024 µL of anhydrous acetonitrile and 25 µL of each reagent was added to each sample (TMT label: peptide [w/w] = 12:1) and mixed briefly by vortexing. The mixture was incubated at room temperature for 1 hr, quenched by the addition of 10 µL of 5% hydroxylamine for 15 min, and then acidified by the addition of 10 µL 10% formic acid. A small aliquot (5 µL) from each reaction was desalted on a StageTip, analyzed by LC-MS/MS with a Q Exactive Orbitrap HF (high field), and resulting spectra searched with MaxQuant using its corresponding TMT label as variable modifications on N terminus and lysine. The percentage of peptides with either N-terminal or lysine TMT labels was calculated, indicating the labeling efficiency for each channel. Labeling efficiency was 96% or greater for each channel. To ensure equal amounts of labeled peptides from each channel were mixed together, a two-step mixing strategy was employed; in the first step, a small (~1 µL) and identical volume of peptides from each channel was mixed and analyzed, and the value of the median ratio (defined by the median of the ratios of all peptide intensities of one channel over their corresponding peptide average intensities of all channels) for each channel is determined as the correction factor. In the second step, the rest of the peptides were mixed by adjusting their volume using the correction factors. In this way, median ratios ranging from 0.97 to 1.02 was achieved as previously reported (Erdjument-Bromage et al., 2018; Huang et al., 2017). The final mixture of reaction products from 10 TMT channels were desalted on a Sep-Pak tC18 1 cc Vac Cartridge (Waters, #WAT03820). Eluted peptides were dried by vacuum centrifugation, and stored at -20°C.

Liquid Chromatography-Tandem Mass Spectrometry and Data Analysis—

Online chromatography was performed with a Thermo Easy nLC 1000 ultrahigh-pressure UPLC system (Thermo Fisher Scientific) coupled online to a Q Exactive HF with a NanoFlex source (Thermo Fisher Scientific). Analytical columns (~30 cm long and 75 µm inner diameter) were packed in-house with ReproSil-Pur C18 AQ 3 µM reversed-phase resin (Dr. Maisch GmbH, Ammerbuch-Entringen, Germany). The analytical column was placed in a column heater (Sonation GmbH, Biberach, Germany) regulated to a temperature of 45°C. The TMT peptide mixture was loaded onto the analytical column with buffer A (0.1%

formic acid) at a maximum back-pressure of 300 bar; peptides eluted with a 2-step gradient of 3% to 40% buffer B (100% ACN and 0.1% formic acid) in 180 min and 40% to 90% B in 20 min, at a flow rate of 250 nL/min over 200 min using a 1D online LC-MS2 data-dependent analysis (DDA) method as follows: MS data were acquired using a data-dependent top-10 method, dynamically choosing the most abundant not-yet-sequenced precursor ions from the survey scans (300–1750 Th). Peptide fragmentation was performed via higher energy collisional dissociation with a target value of 1×10^5 ions determined with predictive automatic gain control. Isolation of precursors was performed with a window of 1 Th. Survey scans were acquired at a resolution of 120,000 at m/z 200. Resolution for HCD spectra was set to 60,000 at m/z 200 with a maximum ion injection time of 128 ms. The normalized collision energy was 35. The “underfill ratio” specifying the minimum percentage of the target ion value likely to be reached at the maximum fill time, is defined as 0.1%. Precursor ions with single, unassigned, or seven and higher charge states were excluded from fragmentation selection. Dynamic exclusion time was set at 30 s. Each of the TMT 10plex sample was analyzed in triplicate.

All data were analyzed with the MaxQuant proteomics data analysis workflow (version 1.5.5.1) with the Andromeda search engine (Cox et al., 2011; Tyanova et al., 2016). The type of the group specific analysis was set to “Reporter ion MS2” with “10plex TMT” as isobaric labels for Q Exactive High Field MS2 data. Reporter ion mass tolerance was set to 0.01 Da, with activated Precursor Intensity Fraction (PIF) value set at 0.75. False discovery rate was set to 1% for protein, peptide spectrum match, and site decoy fraction levels. Peptides were required to have a minimum length of eight amino acids and a maximum mass of 4,600 Da. MaxQuant was used to score fragmentation scans for identification based on a search with an allowed mass deviation of the precursor ion of up to 4.5 ppm after time-dependent mass calibration. The allowed fragment mass deviation was 20 ppm. MS2 spectra were used by Andromeda within MaxQuant to search the Uniprot mouse database (01092015; 16,699 entries) combined with 262 common contaminants. Enzyme specificity was set as C-terminal to arginine and lysine, and a maximum of two missed cleavages were allowed. Carbamidomethylation of cysteine was set as a fixed modification and N-terminal protein acetylation, deamidated (N, Q) and oxidation (M) as variable modifications. The reporter ion intensities were defined as intensities multiplied by injection time (to obtain the total signal) for each isobaric labeling channel summed over all MS/MS spectra matching to the protein group as previously validated (Tyanova et al., 2016). Following MaxQuant analysis, the protein and peptide .txt files were imported into Perseus (version 1.5.6.0) software which was used for the statistical analysis of all the proteins identified. The basic statistics used for significance analysis was the moderated t-statistics (Ritchie et al., 2015). Benjamini-Hochberg correction was used to calculate the adjusted p values.

QUANTIFICATION AND STATISTICAL ANALYSIS

Statistical analyses were performed using OriginPro 9.0 (OriginLab) and Prism (GraphPad Software). For all experiments, the source and value of “n” is stated in the figure legends. For electrophysiological experiments, “n” values for hippocampal slices as well as mice are reported, with “n” = number of animals as the experimental variable used to assess statistical significance. The statistical test for each experiment is reported in the figure legend.

DATA AND CODE AVAILABILITY

The entire proteomic dataset and bioinformatic analysis for the Sam68 interactome shown in Figure 5 is included as Supplementary Tables S1, S2, and S3.

Supplementary Material

Refer to Web version on PubMed Central for supplementary material.

ACKNOWLEDGMENTS

This work is supported by NIH grants R01-AG039521 to B.A.J., R01-MH081935 and R01-DA17392 to P.E.C., and F31-NS073200 and T32-GM007288 to M.E.K.; NIH, NINDS P30-NS050276 and the National Center for Research Resources (S10-RR027990) to T.A.N.; NIH R01-MH49159 and Shiley Marcos Endowment Funds to R.M.; and NIH R01-NS083085 to R.H.S. S.R. is funded by CIHR FDN-154303.

REFERENCES

- Aakalu G, Smith WB, Nguyen N, Jiang C, and Schuman EM (2001). Dynamic visualization of local protein synthesis in hippocampal neurons. *Neuron* 30, 489–502. [PubMed: 11395009]
- Ainsley JA, Drane L, Jacobs J, Kittelberger KA, and Reijmers LG (2014). Functionally diverse dendritic mRNAs rapidly associate with ribosomes following a novel experience. *Nat. Commun* 5, 4510. [PubMed: 25072471]
- Berman RF, Buijsen RA, Usdin K, Pintado E, Kooy F, Pretto D, Pessah IN, Nelson DL, Zalewski Z, Charlet-Bergeurand N, et al. (2014). Mouse models of the fragile X premutation and fragile X-associated tremor/ataxia syndrome. *J. Neurodev. Disord* 6, 25. [PubMed: 25136376]
- Bhakar AL, Dölen G, and Bear MF (2012). The pathophysiology of fragile X (and what it teaches us about synapses). *Annu. Rev. Neurosci* 35, 417–443. [PubMed: 22483044]
- Biever A, Donlin-Asp PG, and Schuman EM (2019). Local translation in neuronal processes. *Curr. Opin. Neurobiol* 57, 141–148. [PubMed: 30861464]
- Bramham CR, Alme MN, Bittins M, Kuipers SD, Nair RR, Pai B, Panja D, Schubert M, Soule J, Tiron A, and Wibrand K (2010). The Arc of synaptic memory. *Exp. Brain Res.* 200, 125–140. [PubMed: 19690847]
- Cajigas JJ, Tushev G, Will TJ, tom Dieck S, Fuerst N, and Schuman EM (2012). The local transcriptome in the synaptic neuropil revealed by deep sequencing and high-resolution imaging. *Neuron* 74, 453–466. [PubMed: 22578497]
- Chawla G, Lin CH, Han A, Shiue L, Ares M Jr., and Black DL (2009). Sam68 regulates a set of alternatively spliced exons during neurogenesis. *Mol. Cell. Biol* 29, 201–213. [PubMed: 18936165]
- Chiu WL, Wagner S, Herrmannová A, Burela L, Zhang F, Saini AK, Valásek L, and Hinnebusch AG (2010). The C-terminal region of eukaryotic translation initiation factor 3a (eIF3a) promotes mRNA recruitment, scanning, and, together with eIF3j and the eIF3b RNA recognition motif, selection of AUG start codons. *Mol. Cell. Biol* 30, 4415–4434. [PubMed: 20584985]
- Chowdhury S, Shepherd JD, Okuno H, Lyford G, Petralia RS, Plath N, Kuhl D, Haganir RL, and Worley PF (2006). Arc/Arg3.1 interacts with the endocytic machinery to regulate AMPA receptor trafficking. *Neuron* 52, 445–459. [PubMed: 17088211]
- Cox J, Neuhauser N, Michalski A, Scheltema RA, Olsen JV, and Mann M (2011). Andromeda: a peptide search engine integrated into the MaxQuant environment. *J. Proteome Res* 10, 1794–1805. [PubMed: 21254760]
- Darnell JC, and Klann E (2013). The translation of translational control by FMRP: therapeutic targets for FXS. *Nat. Neurosci* 16, 1530–1536. [PubMed: 23584741]
- des Georges A, Dhote V, Kuhn L, Hellen CU, Pestova TV, Frank J, and Hashem Y (2015). Structure of mammalian eIF3 in the context of the 43S preinitiation complex. *Nature* 525, 491–495. [PubMed: 26344199]

- Donlin-Asp PG, Rossoll W, and Bassell GJ (2017). Spatially and temporally regulating translation via mRNA-binding proteins in cellular and neuronal function. *FEBS Lett.* 591, 1508–1525. [PubMed: 28295262]
- Dore K, Aow J, and Malinow R (2015). Agonist binding to the NMDA receptor drives movement of its cytoplasmic domain without ion flow. *Proc. Natl. Acad. Sci. USA* 112, 14705–14710. [PubMed: 26553997]
- Erdjument-Bromage H, Huang FK, and Neubert TA (2018). Sample Preparation for Relative Quantitation of Proteins Using Tandem Mass Tags (TMT) and Mass Spectrometry (MS). *Methods Mol. Biol* 1741, 135–149. [PubMed: 29392697]
- Farris S, Lewandowski G, Cox CD, and Steward O (2014). Selective localization of arc mRNA in dendrites involves activity- and translation-dependent mRNA degradation. *J. Neurosci* 34, 4481–4493. [PubMed: 24671994]
- Giorgi C, Yeo GW, Stone ME, Katz DB, Burge C, Turrigiano G, and Moore MJ (2007). The EJC factor eIF4AIII modulates synaptic strength and neuronal protein expression. *Cell* 130, 179–191. [PubMed: 17632064]
- Grange J, Belly A, Dupas S, Trembleau A, Sadoul R, and Goldberg Y (2009). Specific interaction between Sam68 and neuronal mRNAs: implication for the activity-dependent biosynthesis of elongation factor eEF1A. *J. Neurosci. Res* 87, 12–25. [PubMed: 18711726]
- Greer PL, Hanayama R, Bloodgood BL, Mardinly AR, Lipton DM, Flavell SW, Kim TK, Griffith EC, Waldon Z, Maehr R, et al. (2010). The Angelman Syndrome protein Ube3A regulates synapse development by ubiquitinating arc. *Cell* 140, 704–716. [PubMed: 20211139]
- Haas K, Sin WC, Javaherian A, Li Z, and Cline HT (2001). Single-cell electroporation for gene transfer in vivo. *Neuron* 29, 583–591. [PubMed: 11301019]
- Heraud-Farlow JE, and Kiebler MA (2014). The multifunctional Staufen proteins: conserved roles from neurogenesis to synaptic plasticity. *Trends Neurosci.* 37, 470–479. [PubMed: 25012293]
- Hinnebusch AG (2006). eIF3: a versatile scaffold for translation initiation complexes. *Trends Biochem. Sci* 31, 553–562. [PubMed: 16920360]
- Hirokawa N, Niwa S, and Tanaka Y (2010). Molecular motors in neurons: transport mechanisms and roles in brain function, development, and disease. *Neuron* 68, 610–638. [PubMed: 21092854]
- Hodas JJ, Nehring A, Höche N, Sweredoski MJ, Pielot R, Hess S, Tirrell DA, Dieterich DC, and Schuman EM (2012). Dopaminergic modulation of the hippocampal neuropil proteome identified by bioorthogonal noncanonical amino acid tagging (BONCAT). *Proteomics* 12, 2464–2476. [PubMed: 22744909]
- Huang FK, Zhang G, Lawlor K, Nazarian A, Philip J, Tempst P, Dephore N, and Neubert TA (2017). Deep Coverage of Global Protein Expression and Phosphorylation in Breast Tumor Cell Lines Using TMT 10-plex Isobaric Labeling. *J. Proteome Res* 16, 1121–1132. [PubMed: 28102081]
- Huber KM, Kayser MS, and Bear MF (2000). Role for rapid dendritic protein synthesis in hippocampal mGluR-dependent long-term depression. *Science* 288, 1254–1257. [PubMed: 10818003]
- Iijima T, Wu K, Witte H, Hanno-Iijima Y, Glatter T, Richard S, and Scheiffele P (2011). SAM68 regulates neuronal activity-dependent alternative splicing of neurexin-1. *Cell* 147, 1601–1614. [PubMed: 22196734]
- Iijima T, Iijima Y, Witte H, and Scheiffele P (2014). Neuronal cell type-specific alternative splicing is regulated by the KH domain protein SLM1. *J. Cell Biol* 204, 331–342. [PubMed: 24469635]
- Itoh M, Haga I, Li QH, and Fujisawa J (2002). Identification of cellular mRNA targets for RNA-binding protein Sam68. *Nucleic Acids Res.* 30, 5452–5464. [PubMed: 12490714]
- Jackson RJ, Hellen CU, and Pestova TV (2010). The mechanism of eukaryotic translation initiation and principles of its regulation. *Nat. Rev. Mol. Cell Biol* 11, 113–127. [PubMed: 20094052]
- Jakkamsetti V, Tsai NP, Gross C, Molinaro G, Collins KA, Nicoletti F, Wang KH, Osten P, Bassell GJ, Gibson JR, and Huber KM (2013). Experience-induced Arc/Arg3.1 primes CA1 pyramidal neurons for metabotropic glutamate receptor-dependent long-term synaptic depression. *Neuron* 80, 72–79. [PubMed: 24094104]

- Jenks KR, Kim T, Pastuzyn ED, Okuno H, Taibi AV, Bito H, Bear MF, and Shepherd JD (2017). Arc restores juvenile plasticity in adult mouse visual cortex. *Proc. Natl. Acad. Sci. USA* 114, 9182–9187. [PubMed: 28790183]
- Jörntell H, and Hansel C (2006). Synaptic memories upside down: bidirectional plasticity at cerebellar parallel fiber-Purkinje cell synapses. *Neuron* 52, 227–238. [PubMed: 17046686]
- Jung H, Gkogkas CG, Sonenberg N, and Holt CE (2014). Remote control of gene function by local translation. *Cell* 157, 26–40. [PubMed: 24679524]
- Kang H, and Schuman EM (1996). A requirement for local protein synthesis in neurotrophin-induced hippocampal synaptic plasticity. *Science* 273, 1402–1406. [PubMed: 8703078]
- Kano M, Hashimoto K, and Tabata T (2008). Type-1 metabotropic glutamate receptor in cerebellar Purkinje cells: a key molecule responsible for long-term depression, endocannabinoid signalling and synapse elimination. *Philos. Trans. R. Soc. Lond. B Biol. Sci* 363, 2173–2186. [PubMed: 18339599]
- Kemp A, and Manahan-Vaughan D (2008). The hippocampal CA1 region and dentate gyrus differentiate between environmental and spatial feature encoding through long-term depression. *Cereb. Cortex* 18, 968–977. [PubMed: 17702951]
- Kim TK, Hemberg M, Gray JM, Costa AM, Bear DM, Wu J, Harmin DA, Laptewicz M, Barbara-Haley K, Kuersten S, et al. (2010). Widespread transcription at neuronal activity-regulated enhancers. *Nature* 465, 182–187. [PubMed: 20393465]
- Klein ME, Younts TJ, Castillo PE, and Jordan BA (2013). RNA-binding protein Sam68 controls synapse number and local b-actin mRNA metabolism in dendrites. *Proc. Natl. Acad. Sci. USA* 110, 3125–3130. [PubMed: 23382180]
- Klein ME, Castillo PE, and Jordan BA (2015). Coordination between Translation and Degradation Regulates Inducibility of mGluR-LTD. *Cell Rep.* 10, 1459–1466. [PubMed: 25753412]
- Kratz A, Beguin P, Kaneko M, Chimura T, Suzuki AM, Matsunaga A, Kato S, Bertin N, Lassmann T, Vigot R, et al. (2014). Digital expression profiling of the compartmentalized transcriptome of Purkinje neurons. *Genome Res.* 24, 1396–1410. [PubMed: 24904046]
- Lee CS, Dias AP, Jedrychowski M, Patel AH, Hsu JL, and Reed R (2008). Human DDX3 functions in translation and interacts with the translation initiation factor eIF3. *Nucleic Acids Res.* 36, 4708–4718. [PubMed: 18628297]
- Lee JA, Damianov A, Lin CH, Fontes M, Parikshak NN, Anderson ES, Geschwind DH, Black DL, and Martin KC (2016). Cytoplasmic Rbfox1 Regulates the Expression of Synaptic and Autism-Related Genes. *Neuron* 89, 113–128. [PubMed: 26687839]
- Li J, Liu Y, Kim BO, and He JJ (2002). Direct participation of Sam68, the 68-kilodalton Src-associated protein in mitosis, in the CRM1-mediated Rev nuclear export pathway. *J. Virol.* 76, 8374–8382. [PubMed: 12134041]
- Lin Q, Taylor SJ, and Shalloway D (1997). Specificity and determinants of Sam68 RNA binding. Implications for the biological function of K homology domains. *J. Biol. Chem* 272, 27274–27280. [PubMed: 9341174]
- Lukong KE, and Richard S (2003). Sam68, the KH domain-containing superSTAR. *Biochim. Biophys. Acta* 1653, 73–86. [PubMed: 14643926]
- Lukong KE, and Richard S (2008). Motor coordination defects in mice deficient for the Sam68 RNA-binding protein. *Behav. Brain Res* 189, 357–363. [PubMed: 18325609]
- Lyford GL, Yamagata K, Kaufmann WE, Barnes CA, Sanders LK, Copeland NG, Gilbert DJ, Jenkins NA, Lanahan AA, and Worley PF (1995). Arc, a growth factor and activity-regulated gene, encodes a novel cytoskeleton-associated protein that is enriched in neuronal dendrites. *Neuron* 14, 433–445. [PubMed: 7857651]
- Matter N, Herrlich P, and König H (2002). Signal-dependent regulation of splicing via phosphorylation of Sam68. *Nature* 420, 691–695. [PubMed: 12478298]
- Modem S, Badri KR, Holland TC, and Reddy TR (2005). Sam68 is absolutely required for Rev function and HIV-1 production. *Nucleic Acids Res.* 33, 873–879. [PubMed: 15701759]
- Moga DE, Calhoun ME, Chowdhury A, Worley P, Morrison JH, and Shapiro ML (2004). Activity-regulated cytoskeletal-associated protein is localized to recently activated excitatory synapses. *Neuroscience* 125, 7–11. [PubMed: 15051140]

- Mukherjee S, and Manahan-Vaughan D (2013). Role of metabotropic glutamate receptors in persistent forms of hippocampal plasticity and learning. *Neuropharmacology* 66, 65–81. [PubMed: 22743159]
- Nägerl UV, Eberhorn N, Cambridge SB, and Bonhoeffer T (2004). Bidirectional activity-dependent morphological plasticity in hippocampal neurons. *Neuron* 44, 759–767. [PubMed: 15572108]
- Niere F, Wilkerson JR, and Huber KM (2012). Evidence for a fragile X mental retardation protein-mediated translational switch in metabotropic glutamate receptor-triggered Arc translation and long-term depression. *J. Neurosci.* 32, 5924–5936. [PubMed: 22539853]
- Ninomiya K, Ohno M, and Kataoka N (2016). Dendritic transport element of human arc mRNA confers RNA degradation activity in a translation-dependent manner. *Genes Cells* 21, 1263–1269. [PubMed: 27659147]
- Oh WC, Hill TC, and Zito K (2013). Synapse-specific and size-dependent mechanisms of spine structural plasticity accompanying synaptic weakening. *Proc. Natl. Acad. Sci. USA* 110, E305–E312. [PubMed: 23269840]
- Otmakhov N, and Lisman J (2012). Measuring CaMKII concentration in dendritic spines. *J. Neurosci. Methods* 203, 106–114. [PubMed: 21985762]
- Park S, Park JM, Kim S, Kim JA, Shepherd JD, Smith-Hicks CL, Chowdhury S, Kaufmann W, Kuhl D, Ryazanov AG, et al. (2008). Elongation factor 2 and fragile X mental retardation protein control the dynamic translation of Arc/Arg3.1 essential for mGluR-LTD. *Neuron* 59, 70–83. [PubMed: 18614030]
- Paronetto MP, Messina V, Bianchi E, Barchi M, Vogel G, Moretti C, Palombi F, Stefanini M, Geremia R, Richard S, and Sette C (2009). Sam68 regulates translation of target mRNAs in male germ cells, necessary for mouse spermatogenesis. *J. Cell Biol* 185, 235–249. [PubMed: 19380878]
- Plath N, Ohana O, Dammermann B, Errington ML, Schmitz D, Gross C, Mao X, Engelsberg A, Mahlke C, Welzl H, et al. (2006). Arc/Arg3.1 is essential for the consolidation of synaptic plasticity and memories. *Neuron* 52, 437–444. [PubMed: 17088210]
- Popovitchenko T, Thompson K, Viljetic B, Jiao X, Kontonyiannis DL, Kiledjian M, Hart RP, and Rasin MR (2016). The RNA binding protein HuR determines the differential translation of autism-associated FoxP subfamily members in the developing neocortex. *Sci. Rep* 6, 28998. [PubMed: 27383233]
- Ramiro-Cortés Y, and Israely I (2013). Long lasting protein synthesis- and activity-dependent spine shrinkage and elimination after synaptic depression. *PLoS One* 8, e71155. [PubMed: 23951097]
- Rao VR, Pintchovski SA, Chin J, Peebles CL, Mitra S, and Finkbeiner S (2006). AMPA receptors regulate transcription of the plasticity-related immediate-early gene Arc. *Nat. Neurosci* 9, 887–895. [PubMed: 16732277]
- Rappsilber J, Mann M, and Ishihama Y (2007). Protocol for micro-purification, enrichment, pre-fractionation and storage of peptides for proteomics using StageTips. *Nat Protoc.* 2, 1896–1906. [PubMed: 17703201]
- Reymann KG, and Frey JU (2007). The late maintenance of hippocampal LTP: requirements, phases, ‘synaptic tagging’, ‘late-associativity’ and implications. *Neuropharmacology* 52, 24–40. [PubMed: 16919684]
- Richard S, Torabi N, Franco GV, Tremblay GA, Chen T, Vogel G, Morel M, Cléroux P, Forget-Richard A, Komarova S, et al. (2005). Ablation of the Sam68 RNA binding protein protects mice from age-related bone loss. *PLoS Genet.* 1, e74. [PubMed: 16362077]
- Richard S, Vogel G, Huot ME, Guo T, Muller WJ, and Lukong KE (2008). Sam68 haploinsufficiency delays onset of mammary tumorigenesis and metastasis. *Oncogene* 27, 548–556. [PubMed: 17621265]
- Ritchie ME, Phipson B, Wu D, Hu Y, Law CW, Shi W, and Smyth GK (2015). limma powers differential expression analyses for RNA-sequencing and microarray studies. *Nucleic Acids Res.* 43, e47. [PubMed: 25605792]
- Rudinskiy N, Hawkes JM, Betensky RA, Eguchi M, Yamaguchi S, Spires-Jones TL, and Hyman BT (2012). Orchestrated experience-driven Arc responses are disrupted in a mouse model of Alzheimer’s disease. *Nat. Neurosci.* 15, 1422–1429. [PubMed: 22922786]

- Sellier C, Rau F, Liu Y, Tassone F, Hukema RK, Gattoni R, Schneider A, Richard S, Willemsen R, Elliott DJ, et al. (2010). Sam68 sequestration and partial loss of function are associated with splicing alterations in FXTAS patients. *EMBO J.* 29, 1248–1261. [PubMed: 20186122]
- Sossin WS, and Costa-Mattioli M (2019). Translational Control in the Brain in Health and Disease. *Cold Spring Harb. Perspect. Biol.* 11, a032912. [PubMed: 30082469]
- Soulé J, Alme M, Myrum C, Schubert M, Kanhema T, and Bramham CR (2012). Balancing Arc synthesis, mRNA decay, and proteasomal degradation: maximal protein expression triggered by rapid eye movement sleep-like bursts of muscarinic cholinergic receptor stimulation. *J. Biol. Chem.* 287, 22354–22366. [PubMed: 22584581]
- Steward O, and Worley PF (2001). Selective targeting of newly synthesized Arc mRNA to active synapses requires NMDA receptor activation. *Neuron* 30, 227–240. [PubMed: 11343657]
- Steward O, Wallace CS, Lyford GL, and Worley PF (1998). Synaptic activation causes the mRNA for the IEG Arc to localize selectively near activated postsynaptic sites on dendrites. *Neuron* 21, 741–751. [PubMed: 9808461]
- Steward O, Farris S, Pirbhoy PS, Darnell J, and Driesche SJ (2015). Localization and local translation of Arc/Arg3.1 mRNA at synapses: some observations and paradoxes. *Front. Mol. Neurosci.* 7, 101. [PubMed: 25628532]
- Tanenbaum ME, Gilbert LA, Qi LS, Weissman JS, and Vale RD (2014). A protein-tagging system for signal amplification in gene expression and fluorescence imaging. *Cell* 159, 635–646. [PubMed: 25307933]
- Tassone F, Iong KP, Tong TH, Lo J, Gane LW, Berry-Kravis E, Nguyen D, Mu LY, Laffin J, Bailey DB, and Hagerman RJ (2012). FMR1 CGG allele size and prevalence ascertained through newborn screening in the United States. *Genome Med.* 4, 100. [PubMed: 23259642]
- Thompson A, Schäfer J, Kuhn K, Kienle S, Schwarz J, Schmidt G, Neumann T, Johnstone R, Mohammed AK, and Hamon C (2003). Tandem mass tags: a novel quantification strategy for comparative analysis of complex protein mixtures by MS/MS. *Anal. Chem.* 75, 1895–1904. [PubMed: 12713048]
- Tyanova S, Temu T, and Cox J (2016). The MaxQuant computational platform for mass spectrometry-based shotgun proteomics. *Nat. Protoc.* 11, 2301–2319. [PubMed: 27809316]
- Van Driesche SJ, and Martin KC (2018). New frontiers in RNA transport and local translation in neurons. *Dev. Neurobiol.* 78, 331–339. [PubMed: 29314718]
- Wang XB, Yang Y, and Zhou Q (2007). Independent expression of synaptic and morphological plasticity associated with long-term depression. *J. Neurosci.* 27, 12419–12429. [PubMed: 17989307]
- Wang DO, Kim SM, Zhao Y, Hwang H, Miura SK, Sossin WS, and Martin KC (2009). Synapse- and stimulus-specific local translation during long-term neuronal plasticity. *Science* 324, 1536–1540. [PubMed: 19443737]
- Wang C, Han B, Zhou R, and Zhuang X (2016). Real-Time Imaging of Translation on Single mRNA Transcripts in Live Cells. *Cell* 165, 990–1001. [PubMed: 27153499]
- Wang MW, Pfeiffer BE, Nosyreva ED, Ronesi JA, and Huber KM (2008). Rapid translation of Arc/Arg3.1 selectively mediates mGluR-dependent LTD through persistent increases in AMPAR endocytosis rate. *Neuron* 59, 84–97. [PubMed: 18614031]
- Wu B, Buxbaum AR, Katz ZB, Yoon YJ, and Singer RH (2015). Quantifying Protein-mRNA Interactions in Single Live Cells. *Cell* 162, 211–220. [PubMed: 26140598]
- Wu B, Eliscovich C, Yoon YJ, and Singer RH (2016). Translation dynamics of single mRNAs in live cells and neurons. *Science* 352, 1430–1435. [PubMed: 27313041]
- Yoon YJ, Wu B, Buxbaum AR, Das S, Tsai A, English BP, Grimm JB, Lavis LD, and Singer RH (2016). Glutamate-induced RNA localization and translation in neurons. *Proc. Natl. Acad. Sci. USA* 113, E6877–E6886. [PubMed: 27791158]
- Younts TJ, Monday HR, Dudok B, Klein ME, Jordan BA, Katona I, and Castillo PE (2016). Presynaptic Protein Synthesis Is Required for Long-Term Plasticity of GABA Release. *Neuron* 92, 479–492. [PubMed: 27764673]

- Zappulo A, van den Bruck D, Ciolli Mattioli C, Franke V, Imami K, McShane E, Moreno-Estelles M, Calviello L, Filipchuk A, Peguero-Sanchez E, et al. (2017). RNA localization is a key determinant of neurite-enriched proteome. *Nat. Commun* 8, 583. [PubMed: 28928394]
- Zhao WW (2013). Intragenic deletion of RBFOX1 associated with neurodevelopmental/neuropsychiatric disorders and possibly other clinical presentations. *Mol. Cytogenet* 6, 26. [PubMed: 23822903]
- Zheng F, Luo Y, and Wang H (2009). Regulation of brain-derived neurotrophic factor-mediated transcription of the immediate early gene Arc by intracellular calcium and calmodulin. *J. Neurosci. Res* 87, 380–392. [PubMed: 18798281]
- Zhou Q, Homma KJ, and Poo MM (2004). Shrinkage of dendritic spines associated with long-term depression of hippocampal synapses. *Neuron* 44, 749–757. [PubMed: 15572107]
- Zoghbi HY, and Bear MF (2012). Synaptic dysfunction in neurodevelopmental disorders associated with autism and intellectual disabilities. *Cold Spring Harb. Perspect. Biol* 4, a009886. [PubMed: 22258914]

Highlights

- Sam68 promotes the localization and translation of Arc mRNA at distal dendrites
- Distinct processes regulate Arc protein synthesis at the soma versus the dendrite
- Sam68 regulates structural and functional plasticity exclusively at distal synapses
- Interactome analysis reveals a role for Sam68 in translation initiation

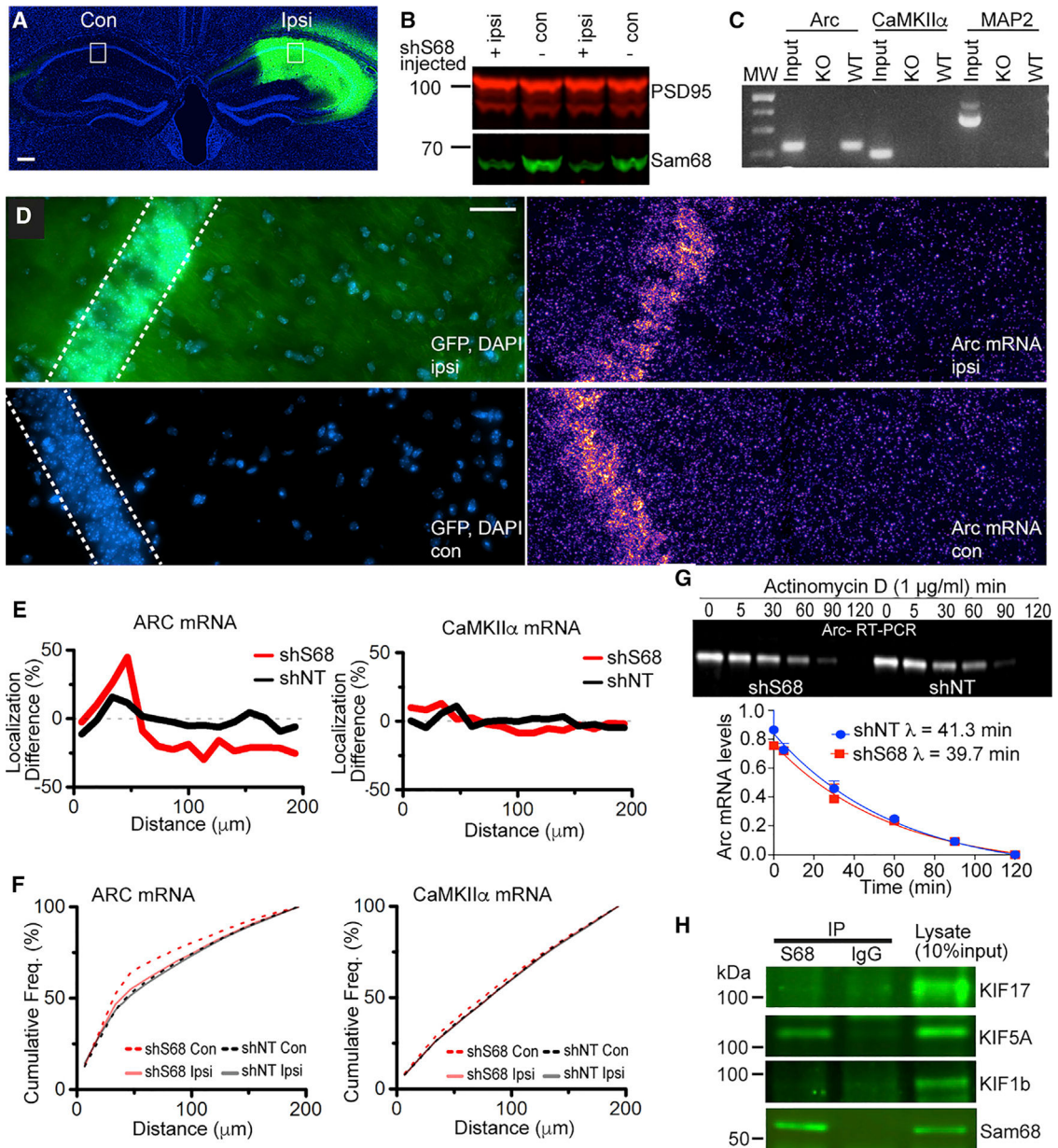


Figure 1. Sam68 Promotes Dendritic Localization of Arc mRNA

(A) Coronal mouse brain section showing ipsilateral (Ipsi) hippocampus injected with shRNA AAVs and GFP and non-injected contralateral (Con) side; 3 weeks post-injection. Scale bar, 200 μ m.

(B) Western blots of dissected hippocampus 3 weeks after injections show shRNAs reduce Sam68 expression. Representative of 3 blots.

(C) RNA IP from WT or Sam68 KO hippocampal lysates shows that Sam68 binds to Arc mRNA but not CaMKII α or MAP2 mRNAs. Representative of 4 RNA IPs.

(D) Magnified views of white boxes from (A) encompassing the *s. pyramidale* (within dashed lines) and *s. radiatum* layers of CA1 (right of *s. pyramidale*). Shown is DAPI (nuclei,

blue), GFP signal, and RNAscope imaging of Arc mRNA in injected (Ipsi) hemisphere (top panels) and uninjected (Con) hemisphere (bottom panels). Scale bar, 50 μ m.

(E) Arc mRNA distribution plotted as percent difference in localization (mRNA enrichment in Ipsi compared to the Con hemisphere) versus distance from the cell body; 0–50 μ m = proximal, >50 μ m = distal. Left panel, shS68 increased Arc mRNA levels in proximal regions and decreased levels in distal regions. No differences were observed with shNT (4 mice per condition; 5 slices per animal, shS68 Ipsi versus Con; Mann-Whitney test, $U = 51$, $p < 0.05$). Right panel, Sam68 knockdown had no effect on CaMKII α mRNA distribution (4 mice per condition; 5 slices per animal, Mann-Whitney test, $U = 93$, $p > 0.05$).

(F) Cumulative frequency distribution plots of data presented in (E), showing a significant difference (two sample Kolmogorov-Smirnov test, KS-test) for Arc mRNA localization (left panel, shS68 Ipsi versus Con, $D = 0.124$, $p < 0.05$; shNT Ipsi versus Con, $D = 0.02$, $p > 0.05$) but not CaMKII α mRNA localization (right panel, shS68 Ipsi versus Con, $D = 0.04$, $p > 0.05$; shNT Ipsi versus Con, $D = 0.04$, $p > 0.05$).

(G) Representative qRT-PCR for Arc mRNA in primary neurons transduced with shS68 or shNT lentiviral shRNAs and treated with the transcriptional inhibitor actinomycin D for the indicated time points (min). Below, qRT-PCR quantitation shows Sam68 knockdown does not affect Arc mRNA degradation. $n = 5$ biological replicates (Mann Whitney test, $U = 15$, $p > 0.05$). Data points represent mean \pm SEM.

(H) Co-immunoprecipitations from cortical brain lysates show Sam68 interacts with kinesin molecular motor KIF5A but not KIF1b or KIF17.

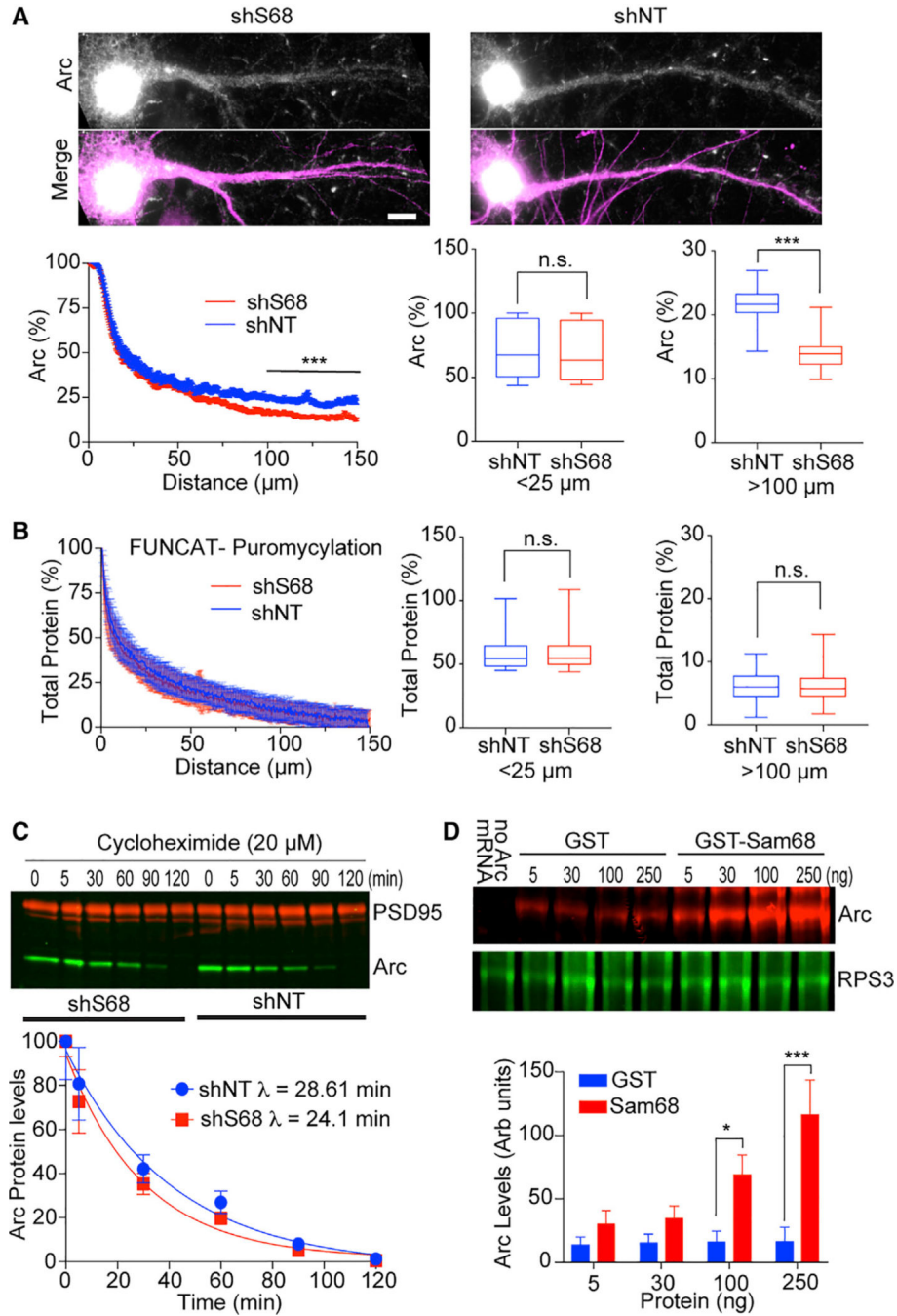


Figure 2. Sam68 Promotes Translation of Arc mRNA at Distal Dendritic Regions

(A) Primary neuronal cultures infected with lentiviral shRNAs and imaged for Arc protein (gray) and MAP2 (magenta) in GFP-positive cells (GFP not shown). Scale bar, 10 μm . Below (left), Arc protein intensity quantified using ImageJ, normalized to levels in the soma (% Arc), and plotted as a function of distance from the cell body. Below (right), Sam68 knockdown significantly reduced Arc protein only in distal dendritic regions (>100 μm). $n = 28$ neurons; three independent experiments (Mann-Whitney, $U = 1166$, $***p < 0.0001$).

(B) Primary neurons infected as in (A) were treated with puromycin (10 μ M) for 15 min and fixed. Loss of Sam68 does not affect global protein synthesis (quantified using anti-puromycin antibodies) proximal or distal to cell bodies. n = 13 neurons; three independent experiments.

(C) Primary neurons were treated with cycloheximide to inhibit translation. Western blots show that loss of Sam68 had no significant effect on Arc protein half-life. n = 3 biological replicates. For (B) and (C), Mann-Whitney U tests give p values >0.05 .

(D) Rabbit-reticulocyte-based *in vitro* translation assay using Arc mRNA and increasing amounts of purified GST or GST-Sam68 protein. Western blots and quantitation below show that Sam68, but not GST, increases Arc translation. RPS3, control ribosomal marker. n = 5 biological replicates. Two-way ANOVA with Sidak post hoc for multiple comparisons, *p < 0.05, ***p < 0.0005. All box and whisker plots indicate mean, 25%–75% percentiles, and min to max range.

Data points in (C) and bar graph in (D) represent mean \pm SEM.

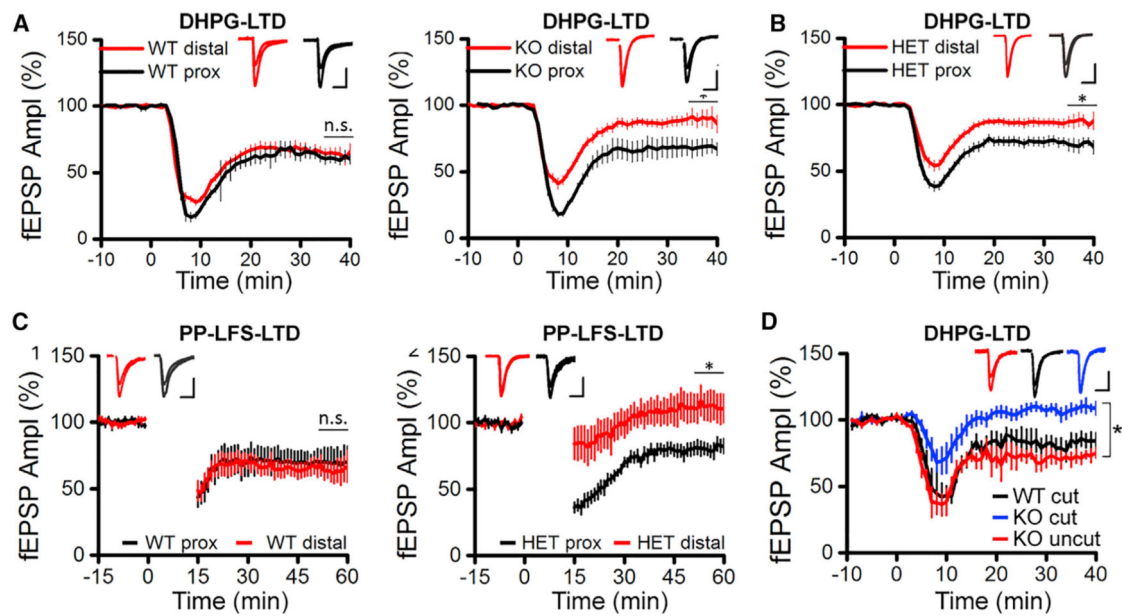


Figure 3. Sam68 Is Required for mGluR-LTD at Distal Dendritic Regions

(A) Field recordings following DHPG-induced mGluR-LTD (DHPG-LTD; 50 μ M, 5 min) in acute hippocampal slices at proximal (\sim 40 μ m from cell body) and distal (\sim 150 μ m from cell body) Schaffer collateral synapses. WT mice show no significant difference between dendritic areas (proximal [33 slices; 9 mice]; distal [32 slices; 9 mice]). Right panel, Sam68 KO mice show significantly impaired DHPG-LTD at distal (17 slices; 4 mice) but not proximal synapses (17 slices; 4 mice).

(B) HET Sam68 KO mice show similar deficits at distal (15 slices; 5 mice) but not proximal synapses (15 slices; 5 mice).

(C) Left panel, WT mice show no significant difference in the magnitude of synaptically induced paired-pulse LFS-LTD (900 pulses; 1Hz; 15 min, 50-ms paired-pulse interval) between proximal inputs (8 slices; 4 mice) and distal inputs (8 slices; 4 mice). Right panel, In Sam68 HET mice, synaptically induced LTD was impaired at distal (8 slices; 4 mice) but not proximal synapses (8 slices; 4 mice).

(D) Field recordings in acute hippocampal slices show that transection of the cell-body layer in Sam68 KO slices (KO cut; 10 cut slices; 4 mice) abolished the DHPG-LTD observed at proximal synapses in untransected slices (KO uncut; 8 control slices; 4 mice). The magnitude of LTD in transected slices from WT mice was comparable to uncut KO slices (WT cut; 4 slices from 2 mice). One-way ANOVA $F(2,9) = 17.2$, $p < 0.05$; paired comparisons; KO cut versus KO uncut, $p < 0.05$; KO cut versus WT cut, $p < 0.05$; KO uncut versus WT cut, $p > 0.05$). For all experiments, data plotted represent mean \pm SEM, and paired representative traces displayed are for baseline and post-LTD; scale bar represents 0.25 mV, and 10 ms. The average % LTD (from pooled slices per animal) calculated across the last 5 minutes of recording were used for statistical evaluation.

Two-tailed Student's *t* test, * $p < 0.05$ and $n =$ number of animals were used for (A), (B), and (C).

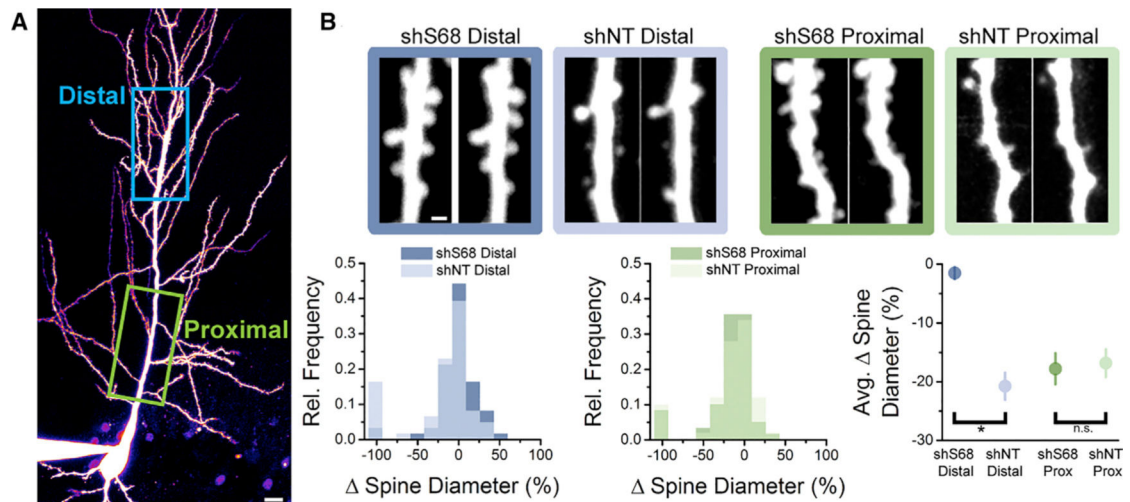


Figure 4. Sam68 Is Required for Structural Plasticity at Distal Dendritic Regions

(A) Two-photon imaging of a hippocampal CA1 pyramidal neuron from organotypic slices electroporated with GFP-containing shRNA expression plasmids. Scale bar, 20 μm .

(B) Top row, dendritic spines from CA1 pyramidal neurons transfected as labeled and from indicated regions. Duos represent baseline and post LTD. Scale bar, 1 μm . Bottom left and middle panels, histograms of changes in spine diameter following DHPG-LTD of distal and proximal dendritic spines. Bottom rightmost panel, scatterplot of average spine diameter decreases following DHPG-LTD as a percentage of baseline diameter. Both proximal and distal spines in neurons expressing shNT show decreased spine diameter post LTD. In neurons expressing shS68, only proximal spines display structural plasticity. Data points represent mean \pm SEM. Paired Student's *t* tests were performed between baseline and post LTD diameters for each condition. *n* = dendritic spines reconstructed; shS68, *n* = 59 proximal and 61 distal; shNT, *n* = 50 proximal and 70 distal, from 4 independent cultures each. **p* < 0.05.

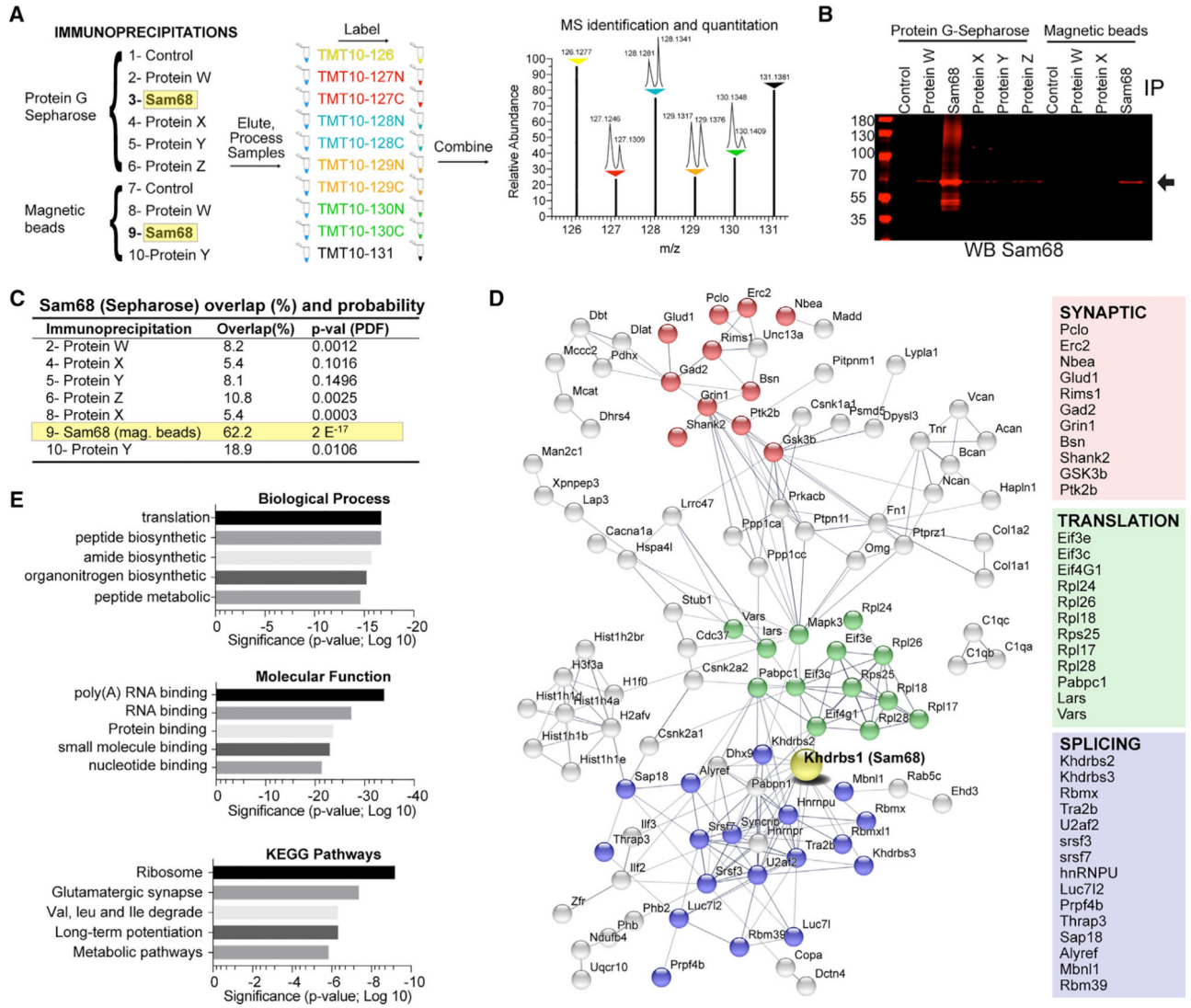


Figure 5. Quantitative Proteomic Analyses of the Sam68 Interactome

(A) IP and isobaric labeling process showing eluted immunocomplexes reacted with unique isobaric tags; 10 plex.

(B) Western blots using 1/100 of the eluted complexes confirm Sam68 immunopurification.

(C) Percent overlap between the Sam68 interactome (Sepharose) and other interactomes with statistics calculated using a hypergeometric means distribution analyses (PDF).

(D) Network analysis for proteins identified in the Sam68 interactome with at least 2 peptides identified and >2-fold enrichment over background. A total of 151 proteins were identified and medium confidence (0.4-String.db) interactions are displayed. A total of 245 interactions (edges) were identified compared to an expected 119 based on random chance.

(E) Ontological analysis of the Sam68 interactome by using 1 detected peptide and at least 1.5-fold enrichment over background identified 534 proteins (see Table S2). The top 5 for indicated classification are listed, showing a strong role for Sam68 in protein translation and RNA metabolism (see Table S3).

KEY RESOURCES TABLE

REAGENT or RESOURCE	SOURCE	IDENTIFIER
Antibodies		
rabbit anti-Sam68	Santa Cruz Biotech	sc-333; RRID: AB_631869
mouse anti-Sam68	Santa Cruz Biotech	sc-136062; RRID: AB_2234147
mouse anti-Puromycin	Millipore	Clone 12D10; RRID: AB_2566826
mouse anti-PSD95	NeuroMab Facility UC Davis	K28/43; RRID: AB_2292909
chicken anti-MAP2	EnCor Biotech	CPCA-MAP2; RRID: AB_2138173
mouse anti-Arc	Santa Cruz Biotech	sc-17839; RRID: AB_626696
rabbit anti-Arc	SYnaptic SYstems, GMBH	156003; RRID: AB_887694
mouse anti-RPS3	Santa Cruz Biotech	sc-376098; RRID: AB_10987662
goat anti-KIF17	Santa Cruz Biotech	N/A; RRID: AB_2131285
mouse anti KIF5A	Santa Cruz Biotech	NKHC1; RRID: AB_2132232
Bacterial and Virus Strains		
pGEX-2T-Sam68	Lin et al., 1997	Addgene plasmid # 17687
pTRIP-Lentiviral Vectors (shS68, shNT)	Linda Van Aelst	N/A
Biological Samples		
Chemicals, Peptides, and Recombinant Proteins		
APV- NMDAR antagonist	NIMH Chemical Synthesis and Drug Supply Program	N/A
Picrotoxin	NIMH Chemical Synthesis and Drug Supply Program	N/A
TTX	NIMH Chemical Synthesis and Drug Supply Program	N/A
NBQX- AMPAR antagonist	NIMH Chemical Synthesis and Drug Supply Program	N/A
Sam68-GST	This paper	N/A
Critical Commercial Assays		
iTaq Universal One-Step RT-qPCR	BioRad	172–5150
rabbit reticulocyte system	Promega	L4960
Deposited Data		
Affinity-based mass spectrometry of Sam68 Interactome	This paper	Tables S1, S2, and S3
Experimental Models: Organisms/Strains		
Sam68 Knockout mice. C57B16J	Stephane Richard (Richard et al., 2005)	
Mice C57B16J	Jackson Labs	CRL-11268
Oligonucleotides		
siRNA targeting sequence: Sam68 (shS68) CGT TAT GAG CAA ACT TGT TAC T	Eurofins	N/A
siRNA control sequence: Nontargeting (shNT) AAG TAT CTA AGC TGT CAC AGA T	Eurofins	N/A
PrimerRT-qPCR- Arc	Eurofins	N/A

REAGENT or RESOURCE	SOURCE	IDENTIFIER
For- ATGAATGGGCCAGCCAAGAA		
PrimerRT-qPCR- Arc	Eurofins	N/A
Rev- TCCTCCTCAGCGTCCACATA		
PrimerRT-qPCR- MAP2	Eurofins	N/A
For- CTGCCGGACCTGAAGAATGT		
PrimerRT-qPCR- MAP2	Eurofins	N/A
Rev- GCTTGGGGACTGTGTGATGA		
PrimerRT-qPCR- CAMKII	Eurofins	N/A
For- GAAGATGTGCGACCCTGGAA		
PrimerRT-qPCR- CAMKII	Eurofins	N/A
Rev- TGCGGATATAGGCGATGCAG		

Author Manuscript

Author Manuscript

Author Manuscript

Author Manuscript